Journal of Mineralogical and Petrological Sciences, Volume 101, page 69–88, 2006

Fayalite rhyolites and a zoned magma chamber of the Paleocene Yakutinskaya volcanic depression in Primorye, Russia

Andrei V. GREBENNIKOV* and Sergey O. MAKSIMOV*

Far East Geological Institute, Prospect Stoletia, 159, 690022 Vladivostok, Russia

During the Late Paleocene, at least five ignimbrite units were emplaced from the Yakutinskaya caldera complex in Primorye, Russia. The erupted ignimbrites show two distinct chemical cycles, believed to represent the "high"-silica and "low"-silica parts of the compositionally zoned magma chamber. Two petrographically distinctive types of rhyolites are distinguishable in each chemical cycle, based on their phenocryst chemistry and silica content: (1) "low"-silica rhyolites with mineral assemblages of quartz, sanidine, plagioclase, ferrohypersthene, ferroaugite ($Ca_{41}Mg_{21}Fe_{38}$), biotite, and hornblende, and (2) "high"-silica rhyolites with a similar mineral assemblage to "low"-silica, but containing more Fe-rich clinopyroxene ($Ca_{44}Mg_2Fe_{54}$) and biotite, and a with lower phenocryst abundance. This difference is related to the variation in chemical composition and temperature of the magma in the zoned magma chamber for each eruption cycle. Rb-Sr mineral-rock isochron ages show that the ignimbrites erupted between 59.7 ± 1.6 and 54.8 ± 2.6 (2σ) Ma (Late Paleocene), and initial $^{87}Sr/^{86}Sr$ ratios are distinct in the different ignimbrite units. The "high"-silica rhyolites show the highest $^{87}Sr/^{86}Sr_I$ ratios (0.70810-0.70738), whereas "low"-silica rhyolites show lower $^{87}Sr/^{86}Sr_I$ ratios (0.70659-0.70724). The compositional zoning of the single magma chamber can be explained by the large-scale mass transport in the liquid phase due to roofward migration and concentration of volatile species.

Keywords: Ignimbrite, Zoned magma chamber, Geochemistry, Sr isotopes, Russia

INTRODUCTION

The Primorsky Krai (Primorye) is located in the East Asian continental margin (Fig. 1), and was formed in the margin of the Bureya-Khanka-Jiamusi continental terrane. The formation of the East Sikhote-Alin volcano-plutonic belt began at the end of the Albian period related to the subduction zone of the Andean-type continental margin (Khanchuk, et. al., 1996). In the late Cretaceous, the volcanic belt formed a part of a transform continental margin of the California-type that resulted from a displacement of the oceanic plate along the continental margin from subduction to sinistral sliding, with a typical manifestation being within-plate magmatism (Khanchuk, et. al., 1999).

The East Sikhote-Alin volcano-plutonic belt stretch-es along the Japan Sea coast, and is 1500 km long and 100 km wide. It is connected with a deep fault system on the boundary of the central Sikhote-Alin. The belt comprises a two-storied structure: the upper part consists of volcanic facies and the lower part consists of dislocated sedimentary rocks. Volcanic complexes were formed during the Cenomanian to Danian. These consist of acid effusive rocks and granite to gabbro complexes. This magmatic activity was terminated by voluminous eruptions of acid magmas, which occurred over the entire area of the belt during the Paleocene. The products of this activity are mainly rhyodacitic to rhyolitic ignimbrites, with associated intrusions exhibiting a similar chemistry (the Bogopolsky igneous complex). The felsic volcanics are mostly preserved within the graben-like structures and/or collapsed calderas.

The Yakutinskaya volcanic depression (YVD) is one such structure, and is situated about 450 km to the northeast of Vladivostok. The depression is located on a junction of the Mesozoic accretionary wedge and turbidite terranes stretching northwest, perpendicular to the characteristic northeast direction of East Sikhote-Alin volcano-plutonic belt. Despite its large size, good state of preservation, and uniqueness, the Yakutinskaya structure has not undergone a comprehensive petrogenetic study before. A study of this structure will provide valuable information on the detailed mechanism of differentiation in silicate melts, and an understanding of the magma system beneath

A.V. Grebennikov, greandr@hotmail.com Corresponding author

the Sikhote-Alin volcanic field.

Detailed studies on the geology of the Bogopolsky igneous complex, bulk rock chemistry, mineral composition, and Sr-isotope ratio of ignimbrites and related rocks have been carried out as a basis for the reconstruction of magma chamber conditions beneath the caldera. The origin of the ignimbrites is discussed in terms of a repeatedly refilled zoned magma chamber model.

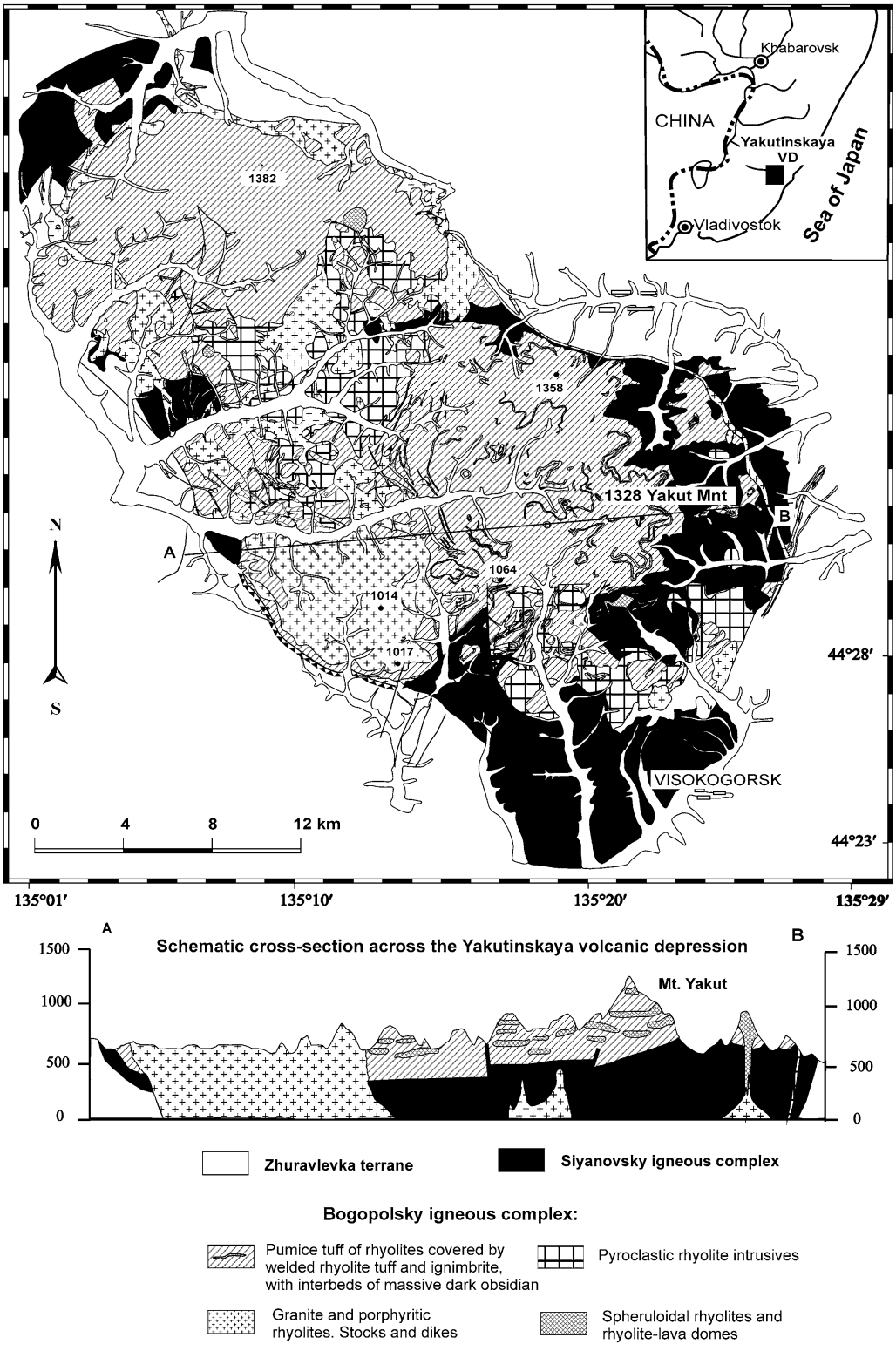

Figure 1. A geological sketch of the Yakutinskaya volcanic depression in Primorye, Russia.

GEOLOGY OF THE YAKUTINSKAYA VOLCANIC DEPRESSION

The YVD is situated towards the continental side of the East Sikhote-Alin volcano-plutonic belt. Mapping around the YVD suggests that the basement rocks of the depression fill are Hauterian-Albian arkosic sandstones interbedded with siltstones. These sediments form part of the Sikhote-Alin flysch association of the Zhuravlevka terrain (Markevich, 1979).

The Yakutinskaya volcanic depression is a large, oval-shaped volcanic massif stretching about 40 km northwest (Fig. 1). It is rimmed by linear and arcuate faults filled with porphyritic rhyolite dikes. The depression was formed by repeated ignimbrite eruptions from several volcanic centers. Older volcanic edifices are deeply eroded to the level of the subsurficial magma chambers, which are filled with porphyritic granite. Younger volcanic constructions are well preserved.

Two caldera formation stages have occurred. During the Maastrichtian period, a large volume of pyroclastics and lavas were emplaced in the depression, forming the Siyanovsky igneous complex. During the Late Paleocene, central constructural edifices of felsic rocks (the Bogopolsky igneous complex) were formed. This younger complex consists of ignimbrites, tuffs, lava domes, and granite. The geology of the YVD has been described by Popov and Grebennikov (1997) and Mikhailov (1989), who divided the Siyanovsky igneous complex into two units: a pyroclastic unit and an overlying lava flow unit. The pyroclastic unit consists of tuffs, welded tuffs, and stratified deposits of rhyodacite to rhyolite composition. Outcrops of these rocks can be seen only in the most eroded parts of the structure. The Maastrichtian age is determined from flora finds in its pyroclastic rocks, as well as the close genetic and spatial connection of its extrusive facies with its stratified sheets (Matyunin et al., 1986). Andesite and dacite lavas are the major components of the lava flow unit. These lavas intrude the pyroclastic unit, and are covered by the Bogopolsky igneous complex.

The Bogopolsky igneous complex is Maastrichtian-Danian in origin, as determined from flora in the tuffaceous silt beds (Matyunin, et al., 1986). As the rocks from the Siyanovsky igneous complex have been highly altered, they are not favorable for petrological examination. Consequently, this study concentrated on the geology of the Bogopolsky igneous complex.

THE BOGOPOLSKY IGNEOUS COMPLEX

This igneous complex consists of both effusive and intrusive facies, predominantly rhyolitic ignimbrites, and tuff layers. A characteristic feature of the Bogopolsky igneous complex is a marked lateral variation and close association of intrusive and extrusive bodies, which comprise the bulk of the complex. The intrusive facies consist of dikes, stocks, and granite batholiths.

The ignimbrite sequences of the Bogopolsky effusives have been studied in detail from a flank of Mount Yakut (Fig. 2). The slope has a stepped profile, and each step corresponds to an individual ignimbrite unit. At least five ignimbrite sequences occur in the depression (hereafter referred to as Ignimbrite (Ign.) 1 to Ign. 5, occurring from the bottom to the top of the geological section). The total thickness of the five units is 600-650 m. Each ignimbrite unit consists fundamentally of three parts: pumice tuff, the ignimbrite body, and tuff beds. Relatively unconsolidated rhyolitic pumice tuff occurs in the lower parts. The pumice tuff is covered by the ignimbrite body, which is unwelded to the welded facies. In the highly welded parts, the ignimbrite is comprised of massive dark obsidian in the Ign. 2 and 4 layers. In the weakly welded parts, fiamme is observed, and the shallow inclination of their

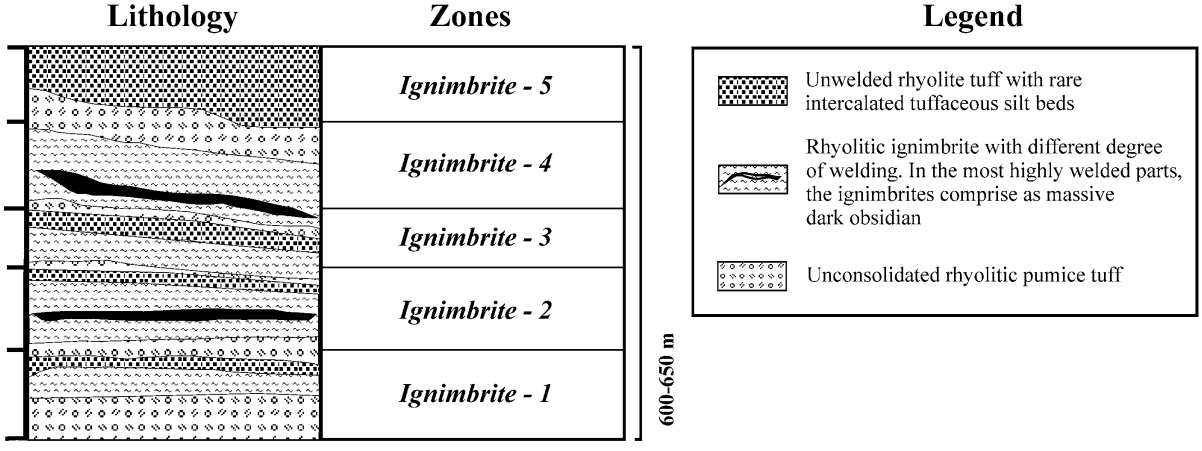

Figure 2. A schematic cross-section of typical ignimbrite sequences of the effusive rocks in the Bogopolskaya suite.

foliations or faces (0–10°) suggests that no significant deformation has occurred after deposition. The ignimbrite sequence is overlain by unwelded rhyolite tuffs, with occasional intercalations of tuffaceous silt beds. The estimated volume of the Yakutinskaya structure ignimbrites is approximately 400 km^3.

Intrusive facies in the complex consist of porphyritic rhyolite dikes and granite stocks. The dikes form ring and linear bodies with an apparent thickness ranging from a few meters to 600 m. In the eastern and northern rims of the YVD, the intrusions form a ring dike belt bounding the volcanic depression from the basement rocks. These dikes also intrude the ignimbrites, which form the depression fill. The contacts are often smooth, and usually dip at high angles into the structure. The thick dikes have porphyritic rhyolite interiors, and grade into fine-grained rhyolite towards their contacts. The thin dikes (1.5–2 m) consist almost entirely of fine-grained rhyolite lavas showing a flow structure. Stretched, crack-filled, or isometric pyroclastic rhyolite intrusions, which grade into granite on the lower hypsometric levels, are also observed in the depression, and are probably facies variations of the underlying granite. Stocks intrude the ignimbrites without exhibiting any effect of strong contact. The contact configurations of these intrusives attest to their sill-like form (Matyunin, 1988). The intrusives are homogeneous, and consist of porphyritic rhyolite. The large-scale stocks consist of granite, which is thought to be a diapir shape.

The rhyolite lavas occur only at the rim of the southern area, and are represented by an array of various scales of oval-shaped lava domes. These domes consist of spheruloidal or vitric rhyolite, some of which grades into the short thick lava flows. Almost all the lava domes are rhyolite, and were active after the emplacement of the voluminous ignimbrites. This suggests that the extrusions originated from a large magma chamber, which now may form a large granite batholith at depth.

PETROGRAPHY AND MINERALOGY OF THE BOGOPOLSKY IGNEOUS COMPLEX

Analytical methods

The mineral compositions were determined using electron probe microanalysis (EPMA) (Model JXA-8800M, JEOL, Japan) located at the Research Center for Coastal Lagoon Environments, Shimane University, Japan, and at the Far East Geological Institute, Russia (Model JXA-5A, JEOL, Japan). The accelerating voltage and sample current were 15 kV and 2×10^{-8}A, respectively. The correction procedure used was that of Bence and Albee (1968). Total iron is reported as FeO.

Because the content of the ferromagnesian mineral, phenocryst, in most of these rocks is low, this phase was separated using heavy liquid and magnetic techniques before mounting and polishing the samples for EPMA. Conventional polished thin sections were also prepared so that the direction and extent of zoning (if present) could be determined.

Effusive facies

Ignimbrites characteristically display horizontal internal structures that are principally due to postdepositional process. In particular, they show varying degrees of welding (Cox et. al., 1979), and this pattern is typical of the ignimbrite of the Yakutinskaya volcanic depression (Fig. 2).

Pumice tuffs are characterized by relatively uniform clast size (about 0.5 mm), and contain angular fragments of quartz (15–20 vol%), K-feldspar (15 vol%), subhedral oligoclase (5 vol%), altered mafic minerals (0.5–1 vol%), all enclosed in a fine-grained ash matrix.

The ignimbrite bodies are composed of sporadic, typically broken crystals, set in, and frequently draped by, glass shards with sinuous or cuspate outlines. They contain phenocrysts of quartz, sanidine, plagioclase, orthopyroxene, clinopyroxene, biotite, hornblende, and olivine (from 5–10 vol% in the lower part, to 30–35 vol% in one of the upper deposits). Not all the minerals occur in each ignimbrite unit.

Quartz (10–15 vol%) shows embayment against the groundmass, which may be interpreted as crystal resorption or be due to rapidly growing crystals enclosing the groundmass material. Many quartz phenocrysts are highly fractured and shattered, and their fragments are slightly shifted relative to each other, which may be the result of an intensive melt decompression during eruption.

Anhedral clasts of sanidine (Or_{70} or Or_{58}; 3–5 vol%) were observed in samples rich in essential olivine (fayalite). Compositional zoning is small. Plagioclase (Pl) phenocrysts (oligoclase) are rare (2–3 vol%), up to 0.8 mm in size, and are euhedral to subhedral. The phenocrysts are twinned, and sometimes show normal zoning with more calcic centers.

Orthopyroxenes (Opx) were found in small amounts (1–2 vol%) in all the mineral separates. Rare orthopyroxene phenocrysts observed in thin sections were predominantly euhedral to subhedral (0.4–0.6 mm), and contained Fe–Ti oxide inclusions. The orthopyroxenes in all the ignimbrites were ferrohypersthenes ($Ca_3Mg_{27}Fe_{70}$, see Table 1).

The clinopyroxenes (less 1 vol%) were generally subhedral (at most, 0.8 mm in size) and typically contained inclusions of apatite and Fe–Ti oxide. Their composition

Table 1. Representative composition of the minerals in the eruptive sequence

	Ignim-1		Ignim-2		Ignim-3		Ignim-4		Dike	Ignim-1		Ignim-2		Ignim-3		Ignim-4		Ignim-5		Dike
	Rhyolite								Dacite	Rhyolite										Dacite
	Opx -c	Opx -r	Opx -c	Opx -r	Opx -c	Opx -r	Opx -c	Opx -r	Opx	Cpx -c	Cpx -r	Cpx -c	Cpx -r	Cpx -c	Cpx -r	Cpx -c	Cpx -r	Cpx -c	Cpx -r	Cpx
SiO_2	48.91	48.41	49.07	48.51	48.90	49.37	48.97	49.03	50.53	49.20	49.35	47.73	48.23	49.60	50.19	47.86	47.78	49.64	49.64	50.05
TiO_2	0.10	0.03	0.04	0.02	0.14	0.15	0.16	0.04	0.28	0.15	0.19	0.31	0.25	0.14	0.14	0.11	0.07	0.09	0.12	0.43
Al_2O_3	0.24	0.22	0.03	0.03	0.05	0.09	0.28	0.28	0.71	0.64	0.74	0.61	0.42	0.45	0.46	0.34	0.27	0.43	0.39	1.16
FeO	40.68	40.90	40.01	39.87	40.62	39.26	41.10	41.31	31.55	22.89	24.34	31.59	29.42	22.00	21.60	30.72	29.83	21.74	21.41	22.45
MnO	0.36	0.43	0.76	0.80	0.76	0.72	0.37	0.44	0.73	0.13	0.23	0.33	0.35	0.19	0.05	0.54	0.49	0.19	0.18	0.50
MgO	8.75	9.37	8.63	9.17	8.93	9.09	8.83	8.79	11.69	6.99	7.03	0.17	0.90	6.92	7.35	0.29	0.42	7.14	7.20	7.63
CaO	1.41	1.42	1.36	1.40	1.38	1.39	1.45	1.35	4.53	18.60	16.81	19.72	19.84	19.59	20.01	19.75	20.03	19.69	19.66	17.63
Na_2O	0.00	0.00	0.00	0.03	0.00	0.02	0.03	0.04	0.11	0.18	0.24	0.28	0.26	0.24	0.24	0.43	0.54	0.20	0.28	0.16
K_2O	0.00	0.00	0.05	0.02	0.05	0.02	0.00	0.00	0.05	0.00	0.00	0.00	0.00	0.00	0.00	0.00	0.00	0.00	0.04	0.03
Total	100.46	100.78	99.95	99.85	100.82	100.11	101.18	101.29	100.18	98.78	98.92	100.75	99.68	99.12	100.03	100.04	99.43	99.12	98.92	100.04
Formulae on basis of 6 oxygens																				
Z																				
Si	1.992	1.972	2.007	1.989	1.988	2.005	1.984	1.986	1.993	1.974	1.980	1.970	1.991	1.980	1.980	1.985	1.990	1.980	1.982	1.970
Al(4)	0.008	0.011	0.000	0.011	0.002	0.004	0.013	0.013	0.007	0.026	0.020	0.030	0.009	0.020	0.020	0.015	0.011	0.020	0.018	0.030
W X Y																				
Al(6)	0.004	0.000	0.002	0.001	0.000	0.000	0.000	0.000	0.025	0.005	0.015	0.000	0.011	0.001	0.001	0.017	0.013	0.000	0.000	0.024
Ti	0.003	0.001	0.001	0.001	0.004	0.005	0.005	0.001	0.008	0.005	0.006	0.010	0.008	0.004	0.004	0.003	0.002	0.003	0.004	0.013
Fe	1.386	1.393	1.369	1.367	1.381	1.333	1.393	1.399	1.041	0.768	0.817	1.091	1.016	0.735	0.712	1.066	1.039	0.725	0.715	0.739
Mn	0.012	0.015	0.026	0.028	0.026	0.025	0.013	0.015	0.025	0.005	0.008	0.012	0.012	0.007	0.002	0.019	0.017	0.007	0.006	0.017
Mg	0.531	0.569	0.526	0.561	0.542	0.550	0.534	0.531	0.687	0.418	0.420	0.010	0.056	0.412	0.432	0.018	0.026	0.425	0.428	0.448
Ca	0.062	0.062	0.060	0.061	0.060	0.061	0.063	0.059	0.191	0.800	0.723	0.872	0.878	0.838	0.846	0.878	0.893	0.841	0.841	0.743
Na	0.000	0.000	0.000	0.003	0.000	0.002	0.002	0.003	0.008	0.014	0.018	0.023	0.021	0.018	0.018	0.034	0.043	0.015	0.022	0.013
K	0.000	0.000	0.003	0.001	0.003	0.001	0.000	0.000	0.003	0.001	0.000	0.000	0.000	0.000	0.000	0.000	0.000	0.000	0.002	0.001
Z	2.00	1.98	2.01	2.00	1.99	2.01	2.00	2.00	2.00	2.00	2.00	2.00	2.00	2.00	2.00	2.00	2.00	2.00	2.00	2.00
WXY	2.00	2.04	1.99	2.02	2.02	1.98	2.01	2.01	1.99	2.01	2.01	2.02	2.00	2.01	2.01	2.04	2.03	2.02	2.02	2.00
Atom percent																				
Ca	3.12	3.05	3.06	3.09	3.04	3.11	3.17	2.95	9.97	40.28	36.88	44.20	45.04	42.23	42.49	44.75	45.63	42.25	42.38	38.51
Mg	26.85	28.12	26.91	28.19	27.31	28.31	26.82	26.69	35.81	21.05	21.44	0.53	2.85	20.76	21.71	0.91	1.32	21.32	21.59	23.19
Fe+Mn	70.03	68.83	70.03	68.73	69.66	68.58	70.01	70.36	54.22	38.67	41.68	55.27	52.11	37.01	35.80	54.34	53.05	36.42	36.03	38.29
Fe#	72.46	71.22	72.62	71.33	72.21	71.16	72.48	72.71	60.78	64.88	66.25	99.07	94.88	64.27	62.30	98.38	97.61	63.28	62.73	62.80

Chemical compositions of the minerals were determined by electron probe microanalyzer (JEOL JXA - 8800M) at the Research Center for Coastal Lagoon Environments, Shimane University, Japan and remeasuared by JXA-5A (for Bi and Amp minerals) at the Far East Geological Institute, Russia.

Note: c, core; r, rim of phenocrysts. Total iron as FeO.

Table 1. (Continued)

	Ignim-1		Ignim-2		Ignim-3		Ignim-4		Ignim-1	Ignim-2		Ignim-3	Ignim-4	
	Rhyolite													
	Bi								Amp					
SiO_2	36.72	36.58	36.84	36.65	36.31	37.30	36.67	36.26	44.13	44.49	43.83	44.53	44.53	45.44
TiO_2	4.72	4.74	4.85	4.57	4.50	4.86	4.63	4.63	1.44	1.89	1.70	2.16	1.81	1.99
Al_2O_3	13.14	13.13	13.25	12.72	12.86	13.06	13.22	13.23	7.70	7.56	7.34	7.90	7.18	7.99
FeO*	27.01	28.39	26.93	29.12	27.35	26.67	27.11	28.80	25.53	25.89	27.23	24.91	26.29	25.46
MnO	0.13	0.12	0.17	0.19	0.16	0.19	0.21	0.24	0.20	0.25	0.44	0.31	0.33	0.59
MgO	6.52	5.83	6.44	4.69	6.55	5.63	6.51	5.19	6.29	6.63	5.00	6.46	6.28	5.56
Na_2O	0.50	0.48	0.51	0.51	0.52	0.46	0.45	0.47	2.31	1.98	2.22	2.01	1.77	2.00
K_2O	9.39	9.61	9.47	9.55	9.93	9.16	9.36	9.39	1.00	1.07	1.08	1.08	0.90	1.08
CaO	0.00	0.00	0.00	0.00	0.00	0.00	0.00	0.00	10.26	10.50	10.46	10.48	10.17	10.84
Cl	0.16	0.16	0.17	0.17	0.18	0.18	0.16	0.20						
F	1.24	1.43	1.25	1.59	1.27	1.58	1.33	1.55						
Total	99.53	100.47	99.88	99.76	99.63	99.09	99.65	99.96	98.86	100.26	99.30	99.84	99.25	100.95
Formulae on basis of 22 oxygens									Formulae on basis of 23 oxygens					
Z														
Si	5.448	5.416	5.448	5.512	5.378	5.609	5.442	5.427	6.735	6.681	6.754	6.716	6.733	6.834
Al(4)	2.298	2.291	2.309	2.254	2.244	2.314	2.311	2.332	1.265	1.319	1.246	1.284	1.267	1.166
Y														
Al(6)	0.000	0.000	0.000	0.000	0.000	0.000	0.000	0.000	0.120	0.019	0.088	0.121	0.012	0.251
Ti	0.526	0.528	0.540	0.517	0.502	0.550	0.517	0.521	0.165	0.213	0.197	0.245	0.206	0.225
Fe	3.350	3.513	3.329	3.661	3.386	3.352	3.363	3.603	3.258	3.251	3.509	3.142	3.324	3.202
Mn	0.016	0.015	0.020	0.025	0.020	0.025	0.026	0.030	0.026	0.032	0.057	0.040	0.042	0.075
Mg	1.441	1.286	1.418	1.050	1.444	1.260	1.439	1.158	1.431	1.484	1.149	1.453	1.416	1.247
X														
Na	0.143	0.136	0.146	0.149	0.150	0.132	0.131	0.136	0.684	0.576	0.663	0.588	0.518	0.583
K	1.775	1.814	1.786	1.832	1.874	1.756	1.771	1.791	0.195	0.205	0.212	0.208	0.174	0.207
Ca	0.000	0.000	0.000	0.000	0.000	0.000	0.000	0.000	1.678	1.689	1.727	1.694	1.647	1.747
Z	7.75	7.71	7.76	7.77	7.62	7.92	7.75	7.76	8.00	8.00	8.00	8.00	8.00	8.00
Y	5.33	5.34	5.31	5.25	5.35	5.19	5.34	5.31	4.88	4.98	4.91	4.88	4.99	4.75
X	1.92	1.95	1.93	1.98	2.02	1.89	1.90	1.93	2.56	2.47	2.60	2.49	2.34	2.54
Fe#	70.03	73.29	70.26	77.83	70.23	72.82	70.19	75.83	69.65	68.87	75.64	68.66	70.39	72.44
fH2	0.059	0.206	-0.516	-0.252	0.054	-0.216	-0.552	-0.364						

	Ignim-1	Ignim-2	Ignim-3	Ignim-4
	Rhyolite			
	Ol			
SiO_2	31.24	30.32	30.02	29.77
TiO_2	0.00	0.00	0.00	0.08
Al_2O_3	0.01	0.00	0.00	0.00
FeO	63.30	67.73	68.52	68.75
MnO	0.57	0.83	0.78	0.81
MgO	4.63	0.84	0.19	0.19
Na_2O	0.00	0.00	0.11	0.00
K_2O	0.01	0.02	0.04	0.05
CaO	0.10	0.13	0.16	0.15
Total	99.86	99.87	99.82	99.80
Formulae on basis of 4 oxygens				
Z				
Si	1.016	1.016	1.013	1.006
Al	0.001	0.000	0.000	0.000
M				
Ti	0.000	0.000	0.000	0.002
Fe	1.723	1.898	1.933	1.944
Mn	0.016	0.024	0.022	0.023
Mg	0.225	0.042	0.009	0.010
Na	0.000	0.000	0.007	0.000
K	0.000	0.001	0.002	0.002
Ca	0.004	0.005	0.006	0.006
Z	1.017	1.016	1.013	1.006
M	1.967	1.969	1.979	1.987
Fe#	88.56	97.86	99.52	99.51

Chemical compositions of the minerals were determined by electron probe microanalyzer (JEOL JXA - 8800M) at the Research Center for Coastal Lagoon Environments, Shimane University, Japan and remeasuared by JXA-5A (for Bi and Amp minerals) at the Far East Geological Institute, Russia.

Note: c, core; r, rim of phenocrysts. Total iron as FeO.

ranged from ferrohedenbergite ($Ca_{44}Mg_2Fe_{54}$) in the Ignimbrite 2 and 4, to ferroaugite ($Ca_{41}Mg_{21}Fe_{38}$) in Ignimbrite 1, 3, and 5 (Table 1). Discrete euhedral grains of ferroaugite ($Ca_{42}Mg_{22}Fe_{36}$) were also found in Ignimbrite 2 and 4.

The fayalite phenocrysts occurred in all ignimbrite units except Ign. 5. In thin sections, up to 1 vol% fayalitic olivine occurred only in rocks with glassy groundmass. The phenocrysts were usually subhedral, up to 0.9 mm, and showed some iddingsitic rim alteration. The average composition was Fa_{89} in Ign. 1 and Fa_{99} in the other units (Table 1).

The hornblende and biotite contents are inversely related to the olivine content. Ignimbrites enriched in olivine (Ign. 2 and 4) contained little hornblende and biotite, whereas rocks depleted in olivine (Ign. 1 and 3) contained higher hornblende and biotite contents. The biotite was brown, iron-rich, and strongly pleochroic. It formed tabular euhedral phenocrysts up to 1.1 mm in length and flaky aggregates in the groundmass. The biotite contents reached 2 vol%. Fiamme in the ignimbrite was characteristically enriched in biotite. In general, as the entire rock silica content increased, the biotite became richer in FeO and MnO, and poorer in MgO and TiO_2. Some biotite grains in Ign. 2 and 4 were more ferruginous than in Ign. 1 and 3 (Table 1). The reaction of biotite with magnetite was common in the more devitrified samples (Ign. 5). This reaction occurred around the edges of the phenocrysts and penetrated along the cleavage planes inside the phenocrysts, suggesting a subsolidus, and hence, a postemplacement reaction.

The amphiboles (0-1.5 vol%) were euhedral or subhedral, and up to 1.4 mm in length. They were calcic, and most could be classified as ferro-edentic hornblende or ferro-hornblende (after the nomenclature of Leake 1978).

The microphenocrysts comprised of ilmenite, and traces of zircon, apatite, and allanite. Small inclusions of ilmenite were also observed in biotite and clinopyroxene. The occurrence of titanomagnetite was extremely rare.

The groundmass was entirely volcanic glass. The glassy matrix in this lithotype had an apparent discontinuous lamination caused by a compaction and welding of the original pumice fragments. The flow texture was characterized by a wavy pattern in which clasts and shards were oriented parallel to the glass flow lines. Characteristically, Ignimbrite units 1 and 3 contained abundant rock fragments, which did not occur in Ignimbrites 2 and 4.

Tuff

A typical tuff facies consisted of phenocrysts and glass shards. The glassy shards were banded and slightly flattened, but were not welded to each other. The glass shards and the phenocrysts were embedded in a devitrified ash matrix. These rocks differed from the ignimbrites, in that they contained greater volumes of phenocrysts (up to 50 vol%), and fewer mafic minerals (about 1 vol%). The mafic minerals were biotite and hornblende, and typically, both were altered. The phenocrysts comprised of quartz (20-25 vol%, 0.6 mm in size and sometimes up to 4 mm), sanidine (15-20 vol%, 2.6 mm in size), and subhedral oligoclase. Ilmenite and rare magnetite were occasionally observed. The groundmass texture is felsitic, and consisted of a mixture of quartz and alkali-feldspar. Sections of fiamme-like quartz aggregates were sometimes observed.

Thin ash-fall tuffs were a minor facies. This rock type was characterized by a vitroclastic structure, with clasts of rounded volcanic glass (7-10 vol%, 0.5 mm in size) and phenocrysts of quartz (5-7 vol%), sanidine (5 vol%), and oligoclase (2-3 vol%). Mafic minerals (0.5-1 vol%) were commonly fully altered and distributed throughout the ash matrix. Allanite (0.6 mm) and ilmenite (0.3 mm) were occasionally observed.

Extrusions (lava domes)

Lava domes commonly consisted of three lava types: rhyolitic obsidian at the margin, and spheruloidal rhyolite lava-filled extrusion vents that sometimes graded into lava flows with a flow structure. All three types were characterized by the presence of phenocrysts (up to 5-7 vol%) of quartz (3-4 vol%), plagioclase An_{17-25} (about 2 vol%), and sanidine Or_{63-68} (about 1 vol%). Their size varied from 1.9 mm (plagioclase) to 3.2 mm (sanidine). Allanite and ilmenite were occasionally observed. The rhyolites showed spherulitic, felsitic, cryptocrystalline, and flow textures. The rhyolitic obsidians were commonly black or sometimes green in hand-held samples, with the glassy groundmass showing a perlitic fracturing that was sometimes emphasized by chloritic margins. Rhyolite lavas with spherulitic texture were characterized by their greater phenocryst content (up to 10 vol%), more sanidine than plagioclase, and felsitic cryptocrystalline groundmass. The plagioclase phenocrysts were frequently leached. The most common occurrence of spherulitic texture was as radiatative aggregates of acicular alkali feldspars with interstitial glass, which commonly enclosed microphenocrysts of quartz, sanidine, and plagioclase. Quartz was also present, resulting in an intergrowth texture. The lava flows showed flow, felsitic, and cryptocrystalline textures. These consisted of phenocrysts of rounded quartz (3-4 vol%, 1.4 mm), sanidine-Or_{59-61} (5-6 vol%, 2.2 mm), and subhedral sieve-textured plagioclase

crystals (3–5 vol%, 1 mm).

Intrusive facies

The porphyritic rhyolite intrusions showed gradual transitions from megaporphyritic to microphyric rhyolite. The former was characterized by a porphyritic texture (up to 50 vol.% phenocryst) with sanidine (Or_{65}, about 15 vol%, 13–14 mm), albitized plagioclase ($An_{0.1-26}$, about 15 vol%, 3–4 mm), quartz (10–15 vol%, 5–6 mm), biotite (Fe# = 66–70, 5–7 vol%, 1–2 mm), and totally altered pyroxenes (1–2 vol%). Accessory minerals present were hornblende, ilmenite, allanite, and zircon. As the lithology tended to be more of the microphyric rhyolite type, the amount of biotite decreased until it became absent, and the phenocryst size and plagioclase percentage decreased. A gradual transition from phaneritic to aphanitic textures was also observed.

The batholithic and diapiric granites were leucocratic coarse-grained rocks with subhedral-granular texture containing mainly quartz, alkali feldspar, plagioclase, and biotite. Alkali feldspars were the most abundant mineral (up to 55 vol%), occurring as orthoclase-microperthite-Or_{57-58}, which was usually anhedral (2.4–4.4 mm). The plagioclase was commonly subhedral oligoclase (An_{14-18}), but was relatively rare (about 3 vol%). Quartz occurred as small plates or aggregates of grains (1.3–2.2 mm) filling spaces between the other constituents, but could reach 40 vol%. Biotite occurred in two forms: as small euhedral plates (0.5–1.3 mm), and as opacite flakes. The latter consisted chiefly of magnetite dust. The biotite was brown, iron-rich (Fe# = 73–79), strongly pleochroic, and could reach 3 vol%. Orthopyroxene, zircon, allanite, and ilmenite were occasionally observed.

GEOCHEMISTRY

Analytical methods

The major and trace element content of the rock samples and ignimbrite fiamme were determined using X-ray fluorescence spectrometry (XRF), employing a Rigaku Model RIX 2000 XRF located at the Department of Geoscience, Shimane University, Japan. Fresh samples were crushed in a jaw crusher, and pounded in a tungsten carbide pestle, and subsequently ground using an automatic agate mortar. The resulting powders were then dried for a period of 24 h at 110 °C. Glass beads were prepared by fusing 1.8 g of rock powder mixed with 3.6 g of alkali flux. The alkali flux used was an 8:2 mixture of lithium tetraborate ($Li_2B_4O_7$, Merck, USA) and lithium metaborate ($LiBO_2$, Merck, USA), based on the method of Kimura and Yamada (1996).

The reproducibility was checked using several igneous rock reference standards provided by the Geological Survey of Japan (GSJ): Sample JB-1 was a basalt and Sample JG-1 was a granitoid. The results were in good agreement with the recommended values.

To perform Sr isotope analysis, the Sr was extracted a Class-1000 clean room located at the Department of Geoscience, Shimane University, Japan, following the method of Kagami et al. (1982, 1987). Each sample (100 to 150 mg) was decomposed in a sealed Teflon vessel using a mixture of HF, HCl, and HNO_3. The Sr was extracted from the decomposed sample using a column filled with a cation exchange resign (Dowex, Japan AG 50W-X8, 200-400 mesh). The Sr extract was loaded onto a Re filament with HCl. The Sr isotope ratio was measured using a Finnigan, MAT 262 (Japan) thermal ionization mass spectrometer equipped with five collectors, and the $^{87}Sr/^{86}Sr$ ratio normalized to $^{86}Sr/^{88}Sr = 0.1194$ was measured. The Sr isotope ratio for Sample NBS987 was measured five times, and showed a mean ratio of 0.710255 ± 0.000009 (2σ = mean). The Rb and Sr concentrations were determined using isotope dilution, and the age and initial Sr isotope ratio were calculated using the method of York (1969). The data were collated from 100 to 240 measurements, comprising of ten scans of 10-24 blocks. To verify the results, samples with very low Sr contents (biotite and fiamme glass) were measured twice.

Major and trace element chemistry

The volcanic rocks were classified using the total alkali versus silica classification diagram of Le Bas et al. (1986). All data were plotted in the rhyolite field (Fig. 3), and showed a single evolutionary trend from the first to the last erupted units (65-85 wt% of SiO_2). The rhyolitic lava formed a different trend, and showed a slight enrichment in CaO (Table 2). The volcanics were subalkaline in composition, according to the criteria of Miyashiro (1978). The fundamental acid magmatic rocks in YVD belong to the ilmenite series (Ishihara, 1997), and from their geochemical, mineralogical, and isotopic features correspond to S-type ilmenite, according to the classification scheme of Chapell and White (1974). Their mostly normative corundum composition reflects their crustal low-depth origin.

The Bogopolsky ignimbrites were classified into "high"- and "low"-silica populations, with the boundary set at ~ 74% SiO_2 (normalized to 100%, water free). This classification is used hereafter. The mineral composition also supported the use of this classification. "high"-silica ignimbrites (Ign. 2 and 4) commonly contained hedenber-

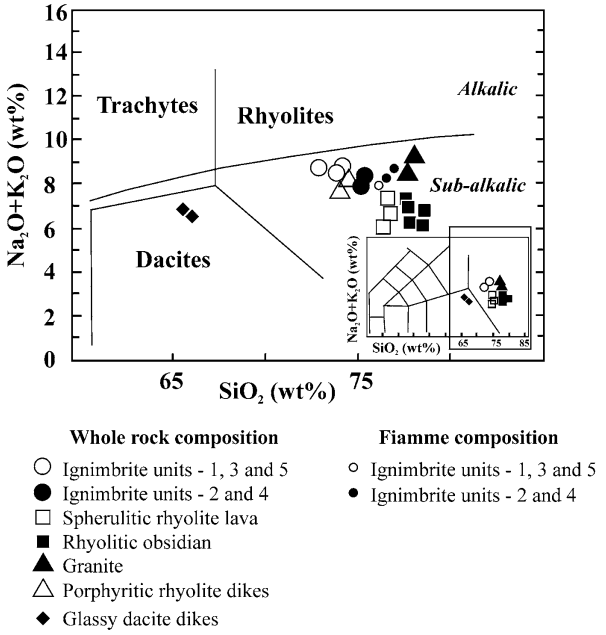

Figure 3. A diagram of the total alkali versus silica classification (Le Bas et al., 1986) for the volcanic rocks of the Yakutinskaya volcanic depression.

gite and biotite crystals, whereas the "low"-silica ignimbrites (Ign. 1, 3, and 5) contained less ferric clinopyroxene and biotite.

From the major and minor element chemistry, both the effusive and intrusive rocks of the Bogopolsky igneous complex can be divided into two groups. The granites and "high"-silica ignimbrites from Ign. 2 and 4, with most the evolved compositions, are characterized by low K/Rb ratios (Fig. 4), and typically, are situated at the end of the whole-rock trend lines. The porphyritic rhyolite dikes and "low"-silica Ign. 1 and 3 show higher Fe, Ti, Ca, and Sr contents than those of the "high"-silica rocks, and also, have higher K/Rb ratios. However, the data for the rhyolite extrusion are an exception. As described above, the extrusion occurs as a glassy rhyolite and a spheruloidal rhyolite at the rim and in the center of a single dome. These erupted during the same eruptive cycle. However, on a K/Rb-Ca/Sr plot (Fig. 4), the rhyolitic obsidians and spheruloidal rhyolites fall into two distinct fields located at opposite ends of the trend, and display a similar chemical contrast as the two groups above.

Sr isotopes and Rb-Sr ages

Data from the Sr isotope analysis and mineral-whole rock Rb-Sr isochron ages are listed in Table 3 and Figure 5, showing that the ignimbrites erupted between 59.7 ± 1.6 and 54.8 ± 2.6 (2σ) Ma (Late Paleocene), from the bottom to the top of the section. These dates are consistent with the stratigraphy, although no age determination was possible for the uppermost ignimbrite in the sequence (Ignimbrite 5) due to the extent of the posteruptive mineral alteration.

According to the Rb-Sr data, a porphyritic rhyolite dike (Sample AV-62) has an Rb-Sr internal isochron age of 55.3 ± 2.8 (2σ) Ma. The age of this intrusion is comparable with the age of the youngest dated ignimbrite (Ignimbrite 4). The lava dome rhyolite (sample AV-59) showed the youngest radiometric age (52.9 ± 3.5 Ma).

It is notable that the "high"-silica rhyolites (Ignimbrite 2 and 4) showed the highest $^{87}Sr/^{86}Sr_I$ value (0.70810-0.70738), and the "low"-silica rhyolites (Ignimbrites 1 and 3) showed the lowest $^{87}Sr/^{86}Sr_I$ values (0.70659-0.70724). Both Sample AV-62 (porphyritic dike) and the dome lava (Sample AV-59) had lower $^{87}Sr/^{86}Sr_I$ ratios in the range 0.70675-0.70692, which is comparable with Ign. 1.

DISCUSSION

Chemical zonation of the ignimbrite magma chamber

The major and trace element data show that the Bogopolsky ignimbrites have a distinct compositional range, and can be divided into two groups based on the data. The first group includes Ignimbrites 1, 3, and 5, and is represented by the "low"-silica rocks, whereas the second group consists of the "high"-silica rhyolite of Ignimbrites 2 and 4. Figure 6 shows the whole-rock enrichment factor diagrams (Hildreth, 1979) that emphasize the contrast in the major and minor elements. The "high"-silica ignimbrites have greater SiO_2, K_2O, Rb, Y, and Nb content and higher Rb/Sr ratio, and therefore, are richer in large ion lithophile (LIL) elements. The "low"-silica and "high"-silica ignimbrites erupted alternatively, and the first ignimbrite (Ign. 1) in the Bogopolsky igneous complex began as a "low"-silica magma eruption.

Similar progressive variations in the bulk composition during large ash-flow eruptions are well documented for the Bandelier Tuff, found in New Mexico, USA (Smith et al., 1966; Smith, 1979), the Bishop Tuff and Long Valley Caldera, from California, USA (Hildreth, 1979; Heumann and Davies, 1997), the Paintbrush Tuff, Nevada, USA (Lipman et al., 1966), the climactic eruption at Crater Lake, Oregon, USA (Williams, 1942), and for the Toba Tuffs, in Sumatra, Indonesia (Chesner, 1998). In most cases, the eruption sequence is characterized by a trend toward less siliceous compositions that are richer in phenocrysts, which according to the above authors reflects zonation within the preeruptive magma chamber. In this

Table 2. Representative composition of the rocks in the eruptive sequence

Element	Ignim-1	Ignim-2	Ignim-3	Ignim-4	W.tuff-5	Ignim-1	Ignim-2	Ignim-4	Extrus.				Dike	Stock		Dike	
	Rhyolite								Rh.-obs.		Spher.rh.		Dacite	Granite		Rhyolite	
	W.rock					Fiamme							W.rock				
SiO_2	71.76	72.49	72.47	71.56	72.16	73.81	74.35	74.34	74.15	74.42	72.32	72.80	64.51	76.80	78.08	72.99	72.41
TiO_2	0.26	0.14	0.28	0.18	0.23	0.13	0.10	0.10	0.11	0.09	0.10	0.09	0.68	0.05	0.08	0.28	0.21
Al_2O_3	13.72	13.22	13.87	13.64	14.36	12.45	12.26	12.15	12.05	12.47	13.11	12.37	14.78	11.53	12.53	13.72	13.40
Fe_2O_3*	2.82	1.66	2.41	1.68	1.99	1.68	1.49	1.44	0.86	1.08	1.72	1.46	7.33	0.76	1.19	2.57	1.96
MnO	0.06	0.05	0.05	0.04	0.03	0.03	0.02	0.02	0.01	0.02	0.02	0.04	0.10	0.02	0.02	0.03	0.05
MgO	0.24	0.16	0.23	0.18	0.20	0.06	0.03	0.01	0.02	0.00	0.29	0.04	0.63	0.14	0.04	0.28	0.19
CaO	1.49	0.88	1.21	0.97	0.84	0.72	0.57	0.53	1.97	1.14	2.29	1.50	3.61	0.30	0.42	1.18	0.72
Na_2O	3.94	3.65	3.47	3.82	3.39	4.12	4.61	4.61	3.73	4.33	2.11	3.14	4.50	4.84	3.51	3.23	4.04
K_2O	4.37	4.21	4.37	3.97	4.71	3.91	3.60	3.67	1.93	2.41	3.08	3.64	2.10	4.43	4.93	4.67	4.04
P_2O_5	0.06	0.02	0.07	0.03	0.01	0.01	0.00	0.00	0.00	0.00	0.00	0.00	0.19	0.05	0.04	0.07	0.04
Total	98.70	96.48	98.43	96.07	97.92	96.92	97.03	96.86	94.83	95.95	95.05	95.09	98.43	98.92	100.85	99.00	97.05
Ba	401.6	n.a.	n.a.	n.a.	n.a.	140.7	90.5	67.6	607.9	444.5	733.1	150.4	1075.1	n.a.	117.1	632.4	1171.4
Ce	164.1	n.a.	n.a.	n.a.	n.a.	79.2	71.5	70.4	91.3	91.7	66.3	64.9	82.9	n.a.	66.4	85.4	69.5
Cr	0.0	n.a.	n.a.	n.a.	n.a.	0.8	1.0	0.9	2.1	0.0	0.0	5.2	3.9	n.a.	0.0	3.6	4.1
Ga	22.5	n.a.	n.a.	n.a.	n.a.	25.6	24.3	25.5	22.6	22.5	23.5	24.4	22.0	n.a.	23.1	21.5	18.6
Nb	17.3	22.0	18.0	17.0	8.0	20.5	20.4	20.7	15.7	19.1	18.9	21.5	14.9	38.0	22.8	13.6	15.3
Ni	1.1	2.0	2.0	2.0	2.0	3.5	2.0	2.0	3.0	3.1	2.3	3.0	3.1	2.0	2.2	3.2	2.4
Pb	25.6	26.0	19.0	30.0	22.0	34.2	34.6	35.0	38.5	315.9	215.3	248.0	30.9	31.0	37.6	23.4	23.3
Rb	183.4	203.0	150.0	191.0	166.0	217.7	252.9	238.5	253.9	212.0	79.4	236.2	136.2	283.0	304.6	153.9	111.7
Sr	208.7	95.0	131.0	72.0	113.0	35.4	7.2	1.3	154.9	62.7	133.9	78.7	356.3	22.0	28.1	107.1	128.8
Th	17.1	n.a.	n.a.	n.a.	n.a.	20.0	18.0	16.0	14.0	15.0	20.0	21.0	7.0	n.a.	25.3	13.0	9.0
V	0.0	10.0	13.0	16.0	24.0	4.1	0.0	0.0	0.0	0.0	3.2	0.0	58.7	3.0	0.0	17.2	3.8
Y	39.2	95.0	45.0	44.0	2.0	43.7	45.7	45.2	65.5	49.4	26.1	45.1	33.7	77.0	52.3	31.4	30.1
Zr	353.7	339.0	251.0	200.0	172.0	184.7	168.6	159.7	169.4	181.7	203.7	176.3	415.7	162.0	130.6	202.5	192.5

Whole rock samples as well as fiamme collected from the ignimbrites were analyzed by X-ray fluorescence spectrometer - Rigaku RIX 2000 at the department of Geoscience, Shimane University, Japan.

Table 2. (Continued)

	Ignim-1		Ignim-2		Ignim-3		Ignim-4		Ignim-1	Ignim-2	Ignim-3	Ignim-4		
	Rhyolite													
	Bi								Amp					
SiO_2	36.72	36.58	36.84	36.65	36.31	37.30	36.67	36.26	44.13	44.49	43.83	44.53	44.53	45.44
TiO_2	4.72	4.74	4.85	4.57	4.50	4.86	4.63	4.63	1.44	1.89	1.70	2.16	1.81	1.99
Al_2O_3	13.14	13.13	13.25	12.72	12.86	13.06	13.22	13.23	7.70	7.56	7.34	7.90	7.18	7.99
FeO*	27.01	28.39	26.93	29.12	27.35	26.67	27.11	28.80	25.53	25.89	27.23	24.91	26.29	25.46
MnO	0.13	0.12	0.17	0.19	0.16	0.19	0.21	0.24	0.20	0.25	0.44	0.31	0.33	0.59
MgO	6.52	5.83	6.44	4.69	6.55	5.63	6.51	5.19	6.29	6.63	5.00	6.46	6.28	5.56
Na_2O	0.50	0.48	0.51	0.51	0.52	0.46	0.45	0.47	2.31	1.98	2.22	2.01	1.77	2.00
K_2O	9.39	9.61	9.47	9.55	9.93	9.16	9.36	9.39	1.00	1.07	1.08	1.08	0.90	1.08
CaO	0.00	0.00	0.00	0.00	0.00	0.00	0.00	0.00	10.26	10.50	10.46	10.48	10.17	10.84
Cl	0.16	0.16	0.17	0.17	0.18	0.18	0.16	0.20						
F	1.24	1.43	1.25	1.59	1.27	1.58	1.33	1.55						
Total	99.53	100.47	99.88	99.76	99.63	99.09	99.65	99.96	98.86	100.26	99.30	99.84	99.25	100.95
Formulae on basis of 22 oxygens									Formulae on basis of 23 oxygens					
Z														
Si	5.448	5.416	5.448	5.512	5.378	5.609	5.442	5.427	6.735	6.681	6.754	6.716	6.733	6.834
Al(4)	2.298	2.291	2.309	2.254	2.244	2.314	2.311	2.332	1.265	1.319	1.246	1.284	1.267	1.166
Y														
Al(6)	0.000	0.000	0.000	0.000	0.000	0.000	0.000	0.000	0.120	0.019	0.088	0.121	0.012	0.251
Ti	0.526	0.528	0.540	0.517	0.502	0.550	0.517	0.521	0.165	0.213	0.197	0.245	0.206	0.225
Fe	3.350	3.513	3.329	3.661	3.386	3.352	3.363	3.603	3.258	3.251	3.509	3.142	3.324	3.202
Mn	0.016	0.015	0.020	0.025	0.020	0.025	0.026	0.030	0.026	0.032	0.057	0.040	0.042	0.075
Mg	1.441	1.286	1.418	1.050	1.444	1.260	1.439	1.158	1.431	1.484	1.149	1.453	1.416	1.247
X														
Na	0.143	0.136	0.146	0.149	0.150	0.132	0.131	0.136	0.684	0.576	0.663	0.588	0.518	0.583
K	1.775	1.814	1.786	1.832	1.874	1.756	1.771	1.791	0.195	0.205	0.212	0.208	0.174	0.207
Ca	0.000	0.000	0.000	0.000	0.000	0.000	0.000	0.000	1.678	1.689	1.727	1.694	1.647	1.747
Z	7.75	7.71	7.76	7.77	7.62	7.92	7.75	7.76	8.00	8.00	8.00	8.00	8.00	8.00
Y	5.33	5.34	5.31	5.25	5.35	5.19	5.34	5.31	4.88	4.98	4.91	4.88	4.99	4.75
X	1.92	1.95	1.93	1.98	2.02	1.89	1.90	1.93	2.56	2.47	2.60	2.49	2.34	2.54
Fe#	70.03	73.29	70.26	77.83	70.23	72.82	70.19	75.83	69.65	68.87	75.64	68.66	70.39	72.44
fH2	0.059	0.206	-0.516	-0.252	0.054	-0.216	-0.552	-0.364						

	Ignim-1	Ignim-2	Ignim-3	Ignim-4
	Rhyolite			
	Ol			
SiO_2	31.24	30.32	30.02	29.77
TiO_2	0.00	0.00	0.00	0.08
Al_2O_3	0.01	0.00	0.00	0.00
FeO	63.30	67.73	68.52	68.75
MnO	0.57	0.83	0.78	0.81
MgO	4.63	0.84	0.19	0.19
Na_2O	0.00	0.00	0.11	0.00
K_2O	0.01	0.02	0.04	0.05
CaO	0.10	0.13	0.16	0.15
Total	99.86	99.87	99.82	99.80
Formulae on basis of 4 oxygens				
Z				
Si	1.016	1.016	1.013	1.006
Al	0.001	0.000	0.000	0.000
M				
Ti	0.000	0.000	0.000	0.002
Fe	1.723	1.898	1.933	1.944
Mn	0.016	0.024	0.022	0.023
Mg	0.225	0.042	0.009	0.010
Na	0.000	0.000	0.007	0.000
K	0.000	0.001	0.002	0.002
Ca	0.004	0.005	0.006	0.006
Z	1.017	1.016	1.013	1.006
M	1.967	1.969	1.979	1.987
Fe#	88.56	97.86	99.52	99.51

Whole rock samples as well as fiamme collected from the ignimbrites were analyzed by X-ray fluorescence spectrometer - Rigaku RIX 2000 at the department of Geoscience, Shimane University, Japan.

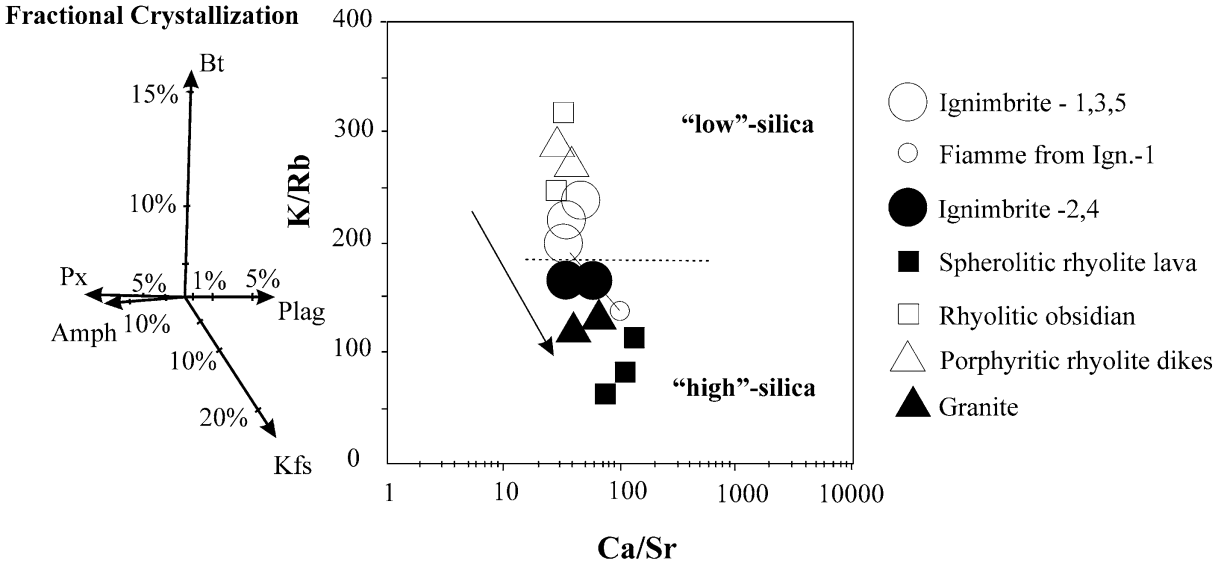

Figure 4. A plot of the Ca/Sr versus K/Rb ratios of the igneous rocks of the Yakutinskaya volcanic depression.

context, Ign. 2 and 3 are thought to have been erupted from a zoned magma chamber, and Ign. 4 and 5 are another pair representing the next eruptive cycle. Periods of 1.5–1.8 My elapsed between these eruptions. Thus, the intervals are relatively uniform between "high"- and "low"-silica ignimbrites, and between the two cycles. As all the ignimbrites lie on a single chemical evolution trend (see Figs. 3 and 4), the magmas are considered to be co-genetic, and so the time required for "low"-silica to "high"-silica evolution is about 1.5–1.6 My. Ignimbrite 1 does not have a "high"-silica counterpart; and may represent the first magma emplacement in the Yakutinskaya volcanic depression.

The ignimbrite glass compositions plotted on the pressure-calibrated An-Or-Q phase diagram of the granite system (Tuttle and Bowen, 1958; Luth et al., 1964; Johannes and Holtz, 1996) suggests confining pressures were between 1.5 and 2.5 kbar (Fig. 7). Assuming a value of the confining pressure of 2 kbar, the Yakutinskaya magmas may have resided in the crust at a depth of approx. 7 km.

Zoned magma chamber: mineralogical and isotopic evidence

The "high"-silica ignimbrites (Ign. 2 and 4) contain phenocrysts of quartz, sanidine (Or_{70}), oligoclase (An_{29}), ferrohypersthene ($Ca_3Mg_{27}Fe_{70}$), olivine (Fa_{99}), and ferrohedenbergite ($Ca_{44}Mg_2Fe_{54}$), with minor biotite ($Annite_{70-77}$), ferro-hornblende, and ilmenite content. Ignimbrites 1, 3, and 5 are characterized by similar mineral assemblages, but contain a greater amount of biotite and hornblende, along with very rare grains (possibly xenocrysts) of olivine Fa_{99} (Fa_{89} in Ign. 1) and ilmenite. Furthermore, crystals of clinopyroxene (Cpx) and biotite are lower in Fe than the "high"-silica ignimbrites are (Fig. 8). The ferrosilite content (Fs) of Cpx also contrasts between the "high" and "low" silica types. The "low"-silica ignimbrites commonly contain Cpx with Fs compositions of Fs_{60-70}, whereas those in the "high"-silica ignimbrites contain Fs_{94-100} (Fig. 8a). The Fe# ratio of the biotites also shows a similar contrast, but with less variation (Fig. 8b). These compositional contrasts in the minerals also support the concept that the "high"- and "low"-silica ignimbrites are from evolved and less evolved magmas, respectively.

Most Yakutinskaya ignimbrites contain ilmenite but no magnetite, and consequently, the Fe-Ti oxide geothermometry cannot be used for temperature determination. A petrographic study of the ignimbrites shows that the clinopyroxene coexists with fayalite in the first erupted units of each cycle (Ignimbrites 2 and 4), and with orthopyroxene in the later flows. The Mg-Fe partitions between coexisting olivine and clinopyroxene (Obata et al., 1974) and between two-pyroxenes (Lindsley, 1983) can be used as an empirical geothermometer. The temperatures were calculated using an estimated pressure 2 kbar using the quartz-ulvospinel-ilmenite-fayalite (QUILF) software program of Frost et al. (1988). This shows that the pre-eruptive temperatures were close to 710 °C for the "high"-silica Ignimbrites 2 and 4, and 780 °C for the "low"-silica Ignimbrites 1 and 3. These temperatures are close to the solidus of water-saturated silicic melts (Johannes and Holtz, 1996). The lower temperature for "high"-silica rhyolitic magma suggests that both thermal and compositional zoning exists in the Yakutinskaya magma chamber.

The observed crystallization of the various ferromag-

Table 3. Chemical composition of the volcanic glasses

	Ignim.-1					Ignim.-4					Extrus.							
	Rhyolite										Rh-obs.				Spher.rh.			
	Fiamme				Matrix	Fiamme		Matrix			Matrix				Shard			
SiO_2	77.70	77.35	77.52	76.88	76.38	75.58	76.57	77.03	76.74	77.49	75.67	74.57	73.30	74.66	77.83	77.53	77.83	77.84
TiO_2	0.06	0.04	0.03	0.06	0.11	0.05	0.06	0.05	0.07	0.03	0.00	0.04	0.04	0.04	0.04	0.02	0.07	0.06
Al_2O_3	12.17	12.46	12.29	12.25	12.43	12.09	12.38	12.45	12.18	12.41	12.32	12.01	12.13	11.91	12.41	12.44	12.22	12.58
FeO*	1.06	0.87	1.23	1.00	1.42	1.12	1.07	1.18	0.99	1.15	0.69	0.33	0.40	0.45	0.87	0.96	1.00	1.00
MnO	0.00	0.00	0.02	0.03	0.07	0.01	0.04	0.03	0.06	0.04	0.01	0.00	0.00	0.01	0.06	0.05	0.12	0.04
MgO	0.00	0.00	0.00	0.00	0.02	0.00	0.02	0.00	0.00	0.00	0.00	0.01	0.00	0.01	0.04	0.04	0.02	0.02
CaO	0.54	0.35	0.55	0.40	0.61	0.29	0.39	0.40	0.46	0.47	0.86	0.91	0.89	0.81	0.28	0.25	0.23	0.21
Na_2O	4.01	4.29	3.90	4.03	3.91	3.51	3.84	3.72	3.63	3.72	2.82	3.00	3.21	3.33	3.19	3.31	3.28	3.38
K_2O	2.98	3.12	3.15	3.06	3.16	2.16	2.20	2.33	2.38	2.26	1.08	1.09	1.12	1.18	2.37	2.34	2.44	2.47
P_2O_5	0.01	0.00	0.00	0.00	0.01	0.03	0.04	0.03	0.00	0.00	0.00	0.00	0.00	0.00	0.00	0.03	0.02	0.04
Total	98.54	98.47	98.69	97.71	98.10	94.84	96.61	97.22	96.52	97.57	93.44	91.96	91.10	92.40	97.09	96.95	97.22	97.63
[Norms]																		
SiO_2	78.85	78.55	78.55	78.68	77.86	79.69	79.25	79.23	79.51	79.42	80.97	81.09	80.46	80.81	80.17	79.96	80.06	79.72
TiO_2	0.06	0.04	0.03	0.06	0.11	0.05	0.06	0.05	0.07	0.03	0.00	0.04	0.04	0.04	0.04	0.02	0.07	0.06
Al_2O_3	12.35	12.65	12.45	12.54	12.67	12.75	12.81	12.81	12.62	12.72	13.19	13.06	13.32	12.88	12.78	12.84	12.57	12.89
FeO*	1.07	0.89	1.25	1.02	1.45	1.18	1.11	1.21	1.03	1.18	0.74	0.36	0.44	0.49	0.90	0.99	1.02	1.02
MnO	0.00	0.00	0.02	0.03	0.07	0.01	0.04	0.03	0.06	0.04	0.01	0.00	0.00	0.01	0.06	0.05	0.12	0.04
MgO	0.00	0.00	0.00	0.00	0.02	0.00	0.02	0.00	0.00	0.00	0.00	0.01	0.00	0.02	0.04	0.04	0.02	0.02
CaO	0.55	0.36	0.56	0.41	0.62	0.31	0.41	0.41	0.48	0.48	0.92	0.99	0.98	0.87	0.29	0.25	0.23	0.22
Na_2O	4.07	4.36	3.95	4.13	3.99	3.70	3.98	3.82	3.76	3.82	3.02	3.26	3.53	3.60	3.28	3.41	3.37	3.46
K_2O	3.03	3.16	3.19	3.14	3.22	2.28	2.28	2.39	2.47	2.32	1.16	1.19	1.23	1.28	2.44	2.41	2.51	2.53
P_2O_5	0.01	0.00	0.00	0.00	0.01	0.03	0.04	0.03	0.00	0.00	0.00	0.00	0.00	0.00	0.00	0.03	0.02	0.04
Total	100.00	100.00	100.00	100.00	100.00	100.00	100.00	100.00	100.00	100.00	100.00	100.00	100.00	100.00	100.00	100.00	100.00	100.00
Fe_2O_3	0.16	0.13	0.19	0.15	0.22	0.18	0.17	0.18	0.15	0.18	0.11	0.05	0.07	0.07	0.13	0.15	0.15	0.15
FeO	1.00	0.83	1.17	0.95	1.35	1.10	1.04	1.14	0.96	1.10	0.69	0.33	0.41	0.46	0.84	0.92	0.96	0.96
Q	41.67	39.68	41.25	41.04	39.99	48.02	45.74	46.08	46.32	46.34	56.41	55.21	52.83	52.72	50.32	49.57	49.52	48.70
C	1.41	1.41	1.50	1.61	1.54	3.71	3.15	3.25	2.88	3.04	5.28	4.61	4.40	3.99	4.21	4.22	3.93	4.15
Or	17.85	18.67	18.79	18.50	18.97	13.47	13.47	14.12	14.54	13.71	6.86	7.03	7.27	7.56	14.42	14.24	14.83	14.95
Ab	34.35	36.81	33.34	34.86	33.68	31.22	33.59	32.32	31.82	32.24	25.55	27.59	29.87	30.46	27.75	28.85	28.52	29.19
An	2.66	1.79	2.78	2.03	3.01	1.34	1.77	1.84	2.38	2.38	4.56	4.91	4.86	4.32	1.44	1.04	1.01	0.83
Hy	1.60	1.35	1.98	1.58	2.30	1.81	1.79	1.90	1.63	1.90	1.19	0.52	0.63	0.79	1.58	1.72	1.80	1.75
Mt	0.23	0.19	0.28	0.22	0.32	0.26	0.25	0.26	0.22	0.26	0.16	0.07	0.10	0.10	0.19	0.22	0.22	0.23
Ilt	0.11	0.08	0.06	0.11	0.21	0.09	0.11	0.09	0.13	0.06	0.00	0.08	0.08	0.08	0.08	0.04	0.13	0.11
Ap	0.02	0.00	0.00	0.00	0.02	0.07	0.09	0.07	0.00	0.00	0.00	0.00	0.00	0.00	0.00	0.07	0.05	0.09
Fe#	100.00	100.00	100.00	100.00	98.93	100.00	98.30	100.00	100.00	100.00	100.00	95.95	100.00	96.82	95.95	95.94	98.04	98.39

Microprobe analyses of glasses (matrix, fiamme, shard of volcanic glass).
All Fe as FeO.

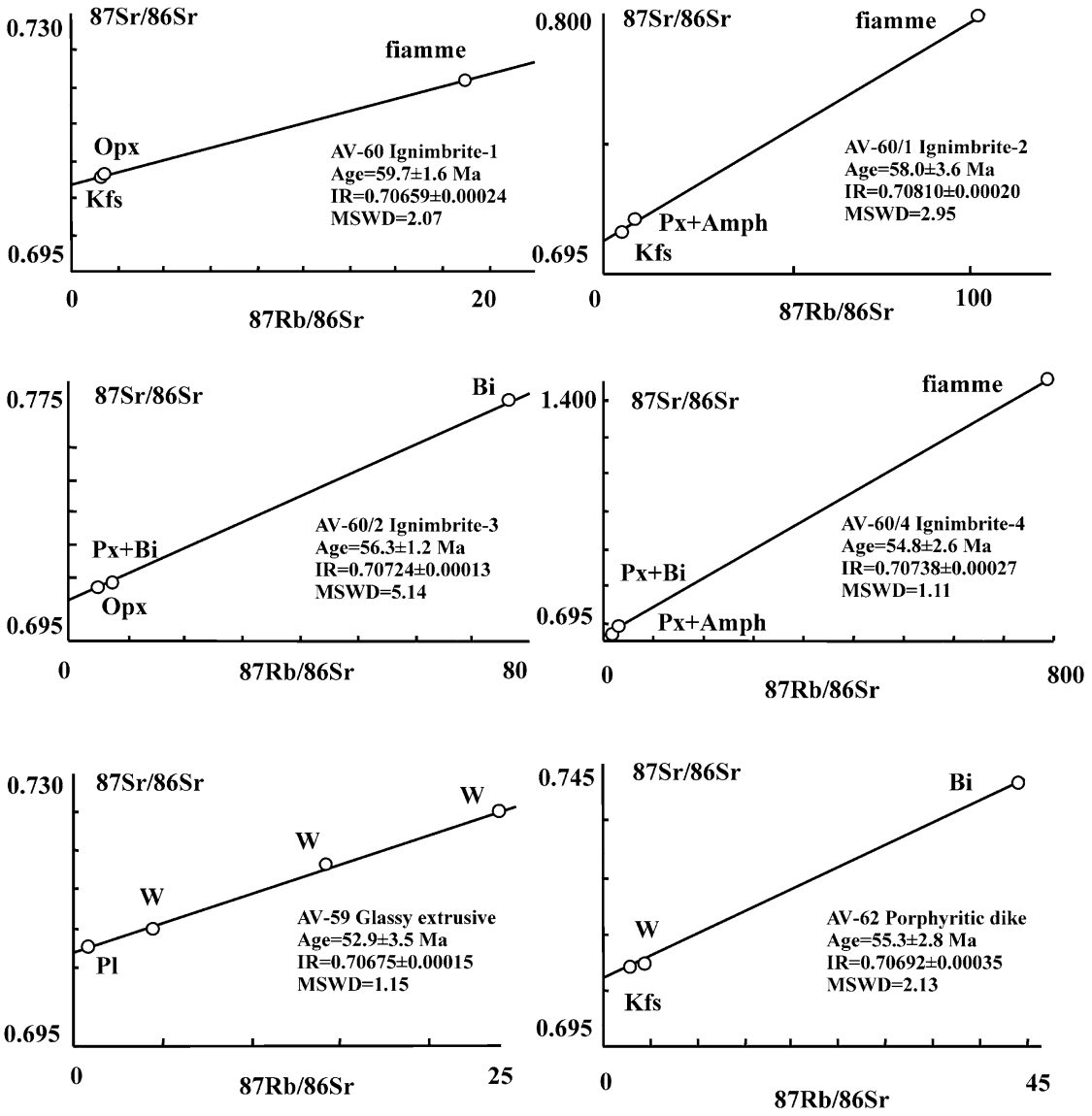

Figure 5. A Rb–Sr isochron diagram for the igneous rocks of the Yakutinskaya volcanic depression. Key: IR, initial Sr isotope ratio; MSWD, mean square weighted deviation. W, whole rock; Bi, biotite; Kfs, feldspar; Pl, plagioclase; Px, pyroxene; Opx, orthopyroxene; Amph, amphibole.

nesian phases may be related to the oxygen fugacity in the "high"-silica rhyolitic magmas (Hildreth, 1981). Moreover, preferential crystallization of iron-rich orthopyroxene over olivine under increasing oxygen fugacity (Carmichael, 1967) suggests that this factor played an important role in the crystallization of the different ferromagnesian phases in the rhyolites. However, single measurements of the oxygen fugacity carried out on microprobe compositions of coexisting minerals (where possible) following the techniques of Anderson and Lindsley (1988), showed f_{O_2} values close to –15.5 log units for Ign. 1 (T = 783 °C) and –16.5 log units for Ign. 2 (T = 706 °C). It is doubtful whether the obtained values fitting the same fayalite-magnetite-quartz (FMQ) buffer curve can explain such differences in mineral crystallization as that observed.

The initial Sr isotope ratios (Table 4) covary with the Fe# in biotite (Fig. 8b). The earliest "low"-silica ignimbrite (Ign. 1) has the lowest $^{87}Sr/^{86}Sr_I$ value, and this is followed by the highest $^{87}Sr/^{86}Sr_I$ value in Ign. 2. Ign.- has a low $^{87}Sr/^{86}Sr_I$ ratio, but the ratio is higher than in Ign. 1. In turn, the "high"-silica Ign. 4 has a slightly greater $^{87}Sr/^{86}Sr_I$ ratio than Ign. 3, but is not as high as in Ign. 2. Ign. 4 is possibly a mixed product between "high" and "low"-silica magmas, and the lower $^{87}Sr/^{86}Sr_I$ ratio could result from such mixing between "high"-silica low-Sr, and "low"-silica high-Sr magmas. This suggests that the high-temperature, "low"-silica end member magmas

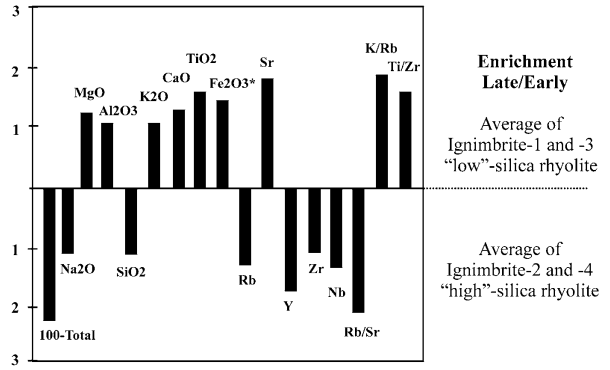

Figure 6. Enrichment factors for selected elements in the ignimbrites and intrusive facies of the Yakutinskaya magma chamber. The factors are calculated by dividing the concentration in the late-erupted samples by the concentration in samples that erupted early in the sequence.

have lower Sr isotope ratios than the low-temperature, "high"-silica magmas do.

The systematic change in bulk chemistry and constituent minerals with geological sequence raises the question of whether the eruptions originated from multiple magma chambers or a single zoned magma chamber. If, by analogy with other ash-flow eruptions, less-silicic magma underlies the "high"-silica bodies, then the eruption of a multiple magma chamber should carry some petrochemical characteristics of higher emplaced magmas. However, there is no evidence for magma mixing between the "high" and "low" silica types in the ignimbrite units. Moreover, Smith (1979) discussed the characteristics of "high-level magma chambers", such as chamber volume and depth, caldera size, and compositional zoning in ignimbrite sheets and magma chambers. He concluded that in small-volume systems, compositional zoning may be rationalized as resulting from two separate magmas from two separate chambers, but in large-volume systems, in which calderas are formed, the two-chamber hypothesis is unrealistic.

The coherence of the chemical and thermal evolution of the rhyolites with time, the similarity of the geochemical characteristics, the unity of the mineralogical features and accessories, and the close grouping on the data plots suggest a single common magmatic reservoir and an

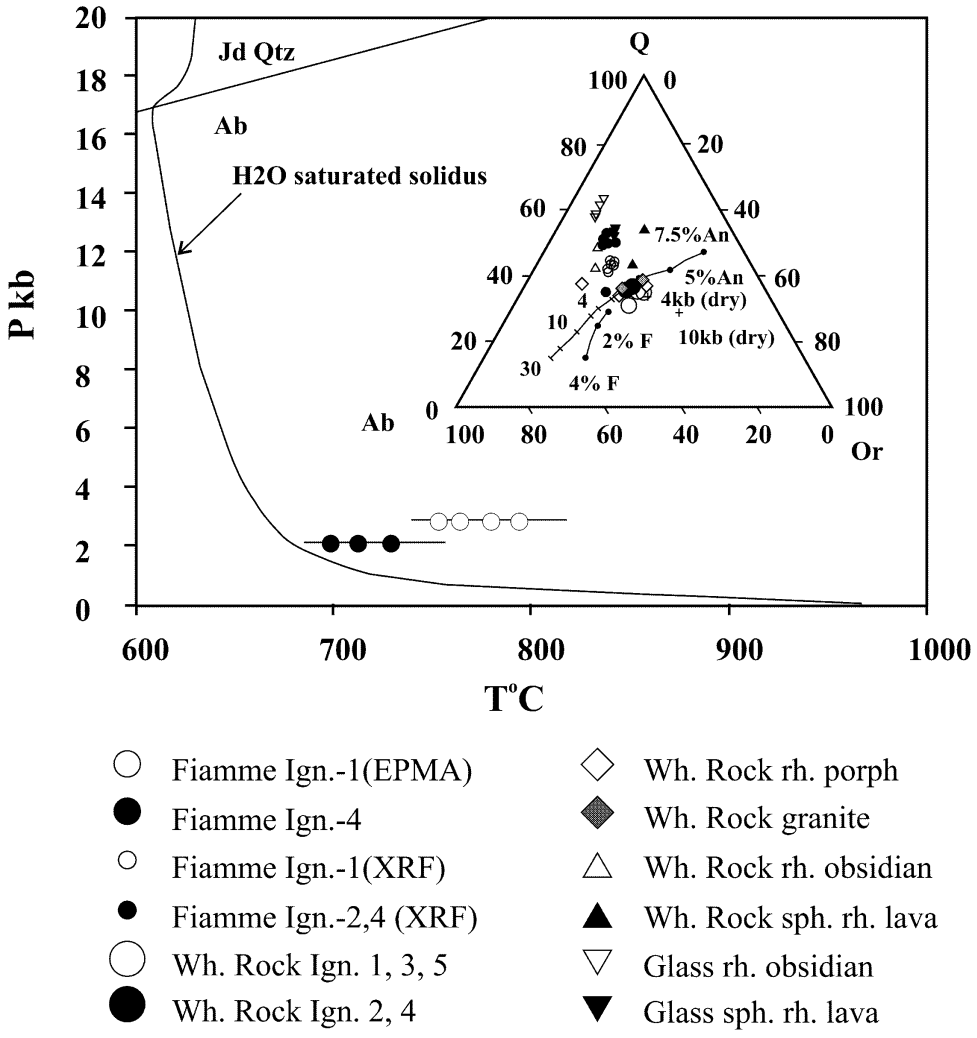

Figure 7. Pressure-temperature diagram showing the beginning of H_2O-saturated melting in the system. Qz-Ab-Or = continuous lines. The inset shows the cotectic lines and composition of the H_2O-saturated minimum and the eutectic in the albite-quartz-orthoclase-H_2O system projected from H_2O onto the Ab-Q-Or plane for pressures of 1 atm and 0.5-30 kbar. Also shown are the minima for the anhydrous system at 4 and 10 kbar pressure (+). Piercing points are shown for the 5% and 7.5% anorthite planes, the 1-4% F minima, and the eutectic for the fluorine-bearing system.

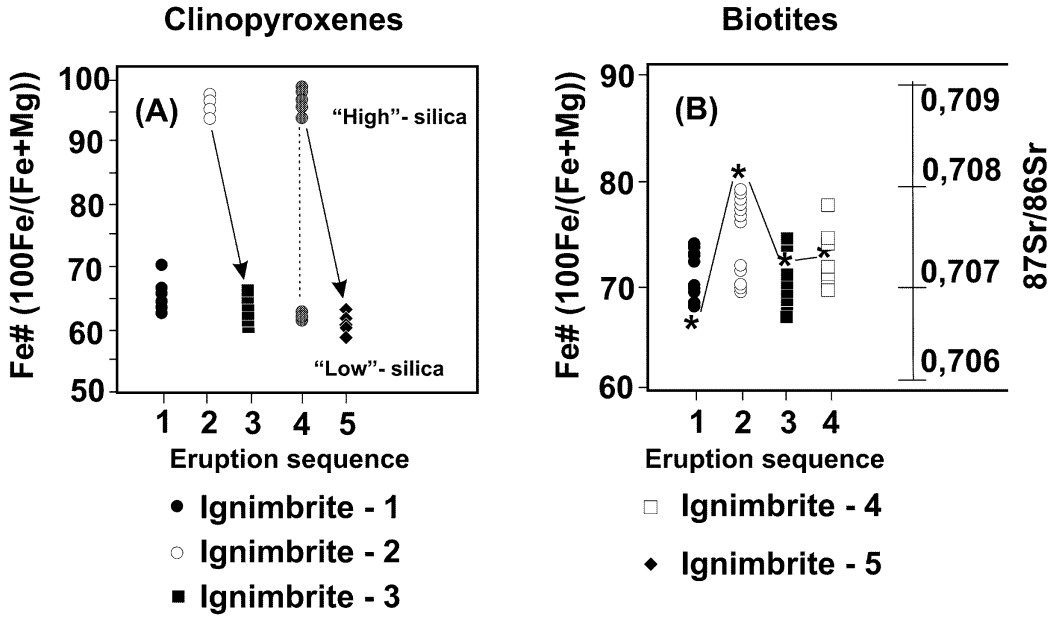

Figure 8. A plot of the composition of the mineral phenocrysts plotted in terms of Fe ratio versus sequence of the rock deposition and Sr isotope initial ratio (∗).

open-system differentiation.

Origin of the compositional zonation

Thus, the Yakutinskaya ignimbrites represent a sequence erupted from different parts of a single evolving magma system, rather than from discrete magma chambers. The processes that may be responsible for the generation of such large volumes of chemically zoned magma (crystallization differentiation, assimilation, magma mixing, liquid immiscibility, progressive partial melting, or thermal contact with primitive magma from the mantle) are fiercely debated in the literature (e.g., see Hildreth, 1979). Most occurrences that show evidence of compositional zonation are attributable to crystal fractionation, most notably the Bishop Tuff (Michael, 1983; Cameron, 1984), Los Humeros Tuffs (Ferriz and Mahood, 1987) and the Toba Tuffs (Chesner, 1998).

Hypothetical models suggest that compositional zonation of silicic magma bodies can develop from double diffusive convection resulting from crystal fractionation (Huppert and Sparks, 1984; Baker and McBirney, 1985; McBirney et al., 1985; Nilson et al., 1985; Turner and Campbell, 1986). To test this hypothesis, least-squares fractionation calculations were carried out on selected samples spanning the compositional range of all the Yakutinskaya units. Vectors showing the nature and magnitude to which different minerals will fractionate K, Ca, Rb, and Sr are shown in Figure 4. The partition coefficients used were from Arth (1976), and Mahood and Hildreth (1983). These calculations suggest that compositional zonation within the YVD units could only be produced by crystal fractionation of the K-feldspar (Kfs).

About 5 wt% fractionation is required to produce a "high"-silica ignimbrite, and 15-20 wt% for an intrusive rocks. About the same amount of Or component (4-5 wt%) is necessary to obtain a "high"-silica composition on the Q-Ab-Or chart (Fig. 7). However, the isotopic data shows significant to pronounced intrasheet differences in the initial $^{87}Sr/^{86}Sr$ ratio within each ignimbrite unit (Table 3 and Fig. 8b). Furthermore, the feldspar phenocrysts (first liquidus phase to be crystallized) are less radiogenic than other associated phenocrysts and groundmass materials (Table 3), and show the same initial isotope ratios in both rock types. Significantly, the initial isotope ratios of the feldspar grains are equal to those of the groundmass materials in Ign. 1 (0.70659). This leads to the conclusion that the silicic magma chamber became zoned immediately after quartz-feldspar crystallization occurred. All these features indicate that the compositional zoning could not have originated by simple crystal settling in the melts.

As mentioned above, "high" SiO_2 samples representing the upper parts of the magma chamber are more radiogenic than samples from the lower parts. Such isotopic zonation could be explained by crustal assimilation, which is more intensive at the roof of large magma chambers (Noble and Hedge, 1969). The highest $^{87}Sr/^{86}Sr_i$ ratio observed in the first "high"-silica (Ign. 2) may represent an intensive assimilation at the roof, and the growth of the

Table 4. Sr isotope ratios and others parameters

Name	Rock	Occur.	Composit.	$^{87}Rb/^{86}Sr$	$^{87}Sr/^{86}Sr$ (P) (2b)	$^{87}Sr/^{86}Sr(I)$	Age, Ma (2b)
AV-59	Extrus.	Rhyolite	Pl	0.529	0.707164 ±11		
AV-59/2A	Extrus.	Rhyolite	Wh.rock	14.315	0.717667 ±34	0,70675 ± 0,00015	52.9 ± 3.5
AV-59/2B	Extrus.	Rhyolite	Wh.rock	23.957	0.724686 ±13		
AV-59/3	Extrus.	Rhyolite	Wh.rock	4.551	0.709972 ±29		
AV-62	Dike	Rhyolite	Bi	41.140	0.741773 ±10		
AV-62	Dike	Rhyolite	Mix(Kfs + w.r)	2.447	0.708861 ±10	0,70692 ± 0,00035	55.3 ± 2.8
AV-62	Dike	Rhyolite	Wh.rock	4.159	0.710175 ± 10		
AV-62	Dike	Rhyolite	Kfs	2.164	0.708409 ± 10		
AV-60/4	Ignim.-4	Rhyolite	Kfs	1.078	0.707435 ± 14		
AV-60/4	Ignim.-4	Rhyolite	Px + Amp	2.741	0.709513 ± 20	0,70738 ± 0,00027	54.8 ± 2.6
AV-60/3a	Ignim.-4	Rhyolite	Fiamme	800.233	1.330234 ± 30		
AV-60/2	Ignim.-3	Rhyolite	Opx	5.400	0.711570 ± 14		
AV-60/2	Ignim.-3	Rhyolite	Bi	76.632	0.768551 ± 31	0,70724 ± 0,00013	56.3 ± 1.2
AV-60/2	Ignim.-3	Rhyolite	Px + Bi	8.055	0.713660 ± 27		
AV-60/2	Ignim.-3	Rhyolite	Kfs		0.708624 ± 27		
AV-60/1	Ignim.-2	Rhyolite	Fiamme	108.635	0.797640 ± 14		
AV-60/1	Ignim.-2	Rhyolite	Px + Amp(Bi)	8.474	0.715185 ± 26	0,70810 ± 0,00020	58.0 ± 3.6
AV-60/1	Ignim.-2	Rhyolite	Px + Amp	5.422	0.712477 ± 22		
AV-60/1	Ignim.-2	Rhyolite	Kfs	3.049	0.709429 ± 22		
AV-60	Ignim.-1	Rhyolite	Opx	1.392	0.707870 ± 14		
AV-60	Ignim.-1	Rhyolite	Kfs	1.306	0.707563 ± 16	0,70659 ± 0,00024	59.7 ± 1.6
AV-60	Ignim.-1	Rhyolite	Fiamme	16.812	0.720845 ± 12		

Sr isotope ratios were measured using a Finnigan MAT 262 thermal ionization mass spectrometer at the department of Geoscience, Shimane University, Japan.

Note: $^{87}Sr/^{86}Sr$ (P) and $^{87}Sr/^{86}Sr$ (I) are the Present and Initial ratios, respectively. *Sr and *Rb in ppm measured by XRF, others by isotope dilution method.

crystal mash may have subsequently reduced the interaction. Noble and Hedge (1969) inferred an assimilation process to account for a similar unusually high initial $^{87}Sr/^{86}Sr$ ratio in five upper Cenozoic ash-flow sheets. Thus, it seems reasonable to hypothesize that much of the variation in the initial $^{87}Sr/^{86}Sr$ ratio (0.70659-0.70810) observed in the Yakutinskaya ignimbrites may be the result of the assimilation of varying amounts of ^{87}Sr enriched upper crustal material. Exposures around the Yakutinskaya depression (Markevich, 1979) suggest that the roof of the magma chamber consisted largely of the Hauterian-Albian arcosic sandstone interbedded with siltstone from the Sikhote-Alin flysch association. Unfortunately, no isotopic data is available from the southern Primorye crystalline basement. However, assimilation of arcosic sandstones and siltstones cannot in any case increase the SiO_2 content (from 72 to 75 wt%) and decrease the Sr content (from 200 to about 80 ppm) in the magmas, due to the content of both elements in the sedimentary rocks of the flysch complex itself (< 67 wt% SiO_2 and > 250 ppm Sr). Thus, there is no evidence for assimilation.

Hildreth (1979) used the thermogravitational convection-diffusion model proposed by Shaw et al. (1976) to explain the repeated establishment of associated thermal, compositional, volatile, and isotopic gradients in large silicic magma chambers. This model permits a diffusional influx of water and some minor components from outside the magma chamber, but its main emphasis is on the combined effect of convective circulation and internal diffusion developing a chemical gradient within the thermal and gravitational field of the magma chamber itself. This model seems most appropriate for the magmatic rocks of the Yakutinskaya volcanic depression.

However, it is difficult to present geological evidence for the co-existence of two magmas within a single and layered magma reservoir in the Yakutinskaya magmatic system, taking into account Pl-Kfs-Opx paragenesis and the similarity of the chemical compositions, especially in terms of alkalinity. The mineralogical differences are firstly expressed in the enrichment of "high"-silica ignimbrites by extreme Fe-rich silicates and their accessory contents compared to Ign. 1. Crystallization of the abnormal high Fe# silicates (Cpx and Ol) should be considered as a disequilibrium subsolidus phase with regards to the transmagmatic Opx grains that occur in all rock types. Their unusually high Fe# cannot be only related to an extremely low oxygen fugacity regime, but may be due to crystallization from a residual, high water-saturated, relatively low-temperature, almost magnesium-free melt that permitted crystallization of fayalite and ferrohedenbergite, even under FMQ buffered conditions. This is the result of the higher fluidization in the roof zone of the system.

The first group has higher Al_2O_3, MgO and CaO contents and a lower SiO_2 content. This is well correlated with the crystalline nature of Group 1 and vitrophyric character of the second group. The chemical composition of the volcanic glasses (Table 3) shows that glassy, fluid enriched melts (Ign. 4) change from having a "potassium"- to a "sodium"-type alkalinity, and the degree of coordination state of Al_2O_3 changes from calcium to alkali. This process is also responsible for the degree of fluid saturation of the system. Taking into account the concordant changes of the chemical composition (K/Na and Rb/Sr ratios, and CaO and SiO_2) between Ignimbrites 1, 3, and 5 and Ignimbrites 2 and 4 eruptions and their fiamme (fluid saturated sections) we propose that the chemical activity character of the silicate system is determined by the mobile behavior of the alkaline elements, and especially Na.

Geologically well-defined zoning-alternation of different fluid saturated flows conditioned by insignificant but regular chemical variations, and most importantly by specific mineralogy, is necessary to relate to the enrichment of definite erupted phases of the "head" column by a fluid, and not with chemical stratification of the melts. Following on from this process, changes will be expressed in regular successive, less fluid saturated explosions.

Such differentiation of rhyolite magma in a high-level magma chamber is formed by a gravitation floating mechanism of a more fluidized, and thus lighter, melt into the apical part of the chamber. According to Lowell (1985) and Nilson et al. (1985) the floating of a fluidized portion of the melt leads to an accumulation of light components near the roof with a geologically significant speed of 10^{-3} km^3/year. It is supposed that due to this process in a geologically short period, the formation of a subsurficial bed that subsequently erupts takes place.

A change in the melt structure caused by an increase in water concentration and depolymerization will give rise to differences in the occupation of water-saturated melt cations compared to a less water-saturated melt (Watson, 1982; Lesher, 1986; Maury and Bizouard, 1974). Variations in the $^{87}Sr/^{86}Sr(I)$ ratios and their rise in "high" silica, more fluidized and low-temperature melts are probably connected not with host rocks assimilation, but with ^{87}Sr self-diffusion into the octahedral melt structure (Watson, 1982; Baker, 1989; Pankhurst, 1969). Thus, the "low"-silica rhyolites of the Yakutinskaya volcanic depression represent the deeper and hotter portion of the magma chamber, whereas the "high"-silica rhyolites are derived from the stratified upper layer of the chamber that grew gradually as the underlying chamber cooled, and differentiated following each new addition of magma. The compositional zonation of the single magma chamber can largely be explained by a large-scale mass transport in the liquid phase due to roofward migration and concentration of volatile species.

CONCLUSIONS

1. At least five ignimbrite units were erupted from the Yakutinskaya magma chamber. The ignimbrites were deposited between 54.8 ± 2.6 and 59.7 ± 1.6 Ma (in the Paleocene). The magma erupted during each successive eruption was compositionally zoned, ranging from "low" silica to "high" silica rhyolite.
2. The composition of the ferromagnesian silicates in the ignimbrite units and their preeruptive temperature varied systematically with stratigraphic sequence. Clinopyroxene occurring in the basal deposits of each member was the richest in Fe and Mn, and the poorest in Mg. The uppermost flows of these units had the most magnesian pyroxenes and the highest preeruptive temperature. These flows originated in the deepest, hottest zone of a single zoned magma chamber. This zone had the lowest Si content in the chamber.
3. The "high"-silica granites and "low"-silica porphyritic rhyolites inherited the geochemical peculiarities of the ignimbrites, and can be regarded as an example of zoned magma chamber rocks exposed at the surface.

ACKNOWLEDGMENTS

Our thanks go to Professor Yoshihiro Sawada for his supervision and assistance, and to Professor Shigeru Iizumi for allowing me the opportunity to undertake Sr

isotope work and his guidance during the analysis. We wish to thank Professor Junichi Kimura and Professor Barry Roser for constructive discussions, reviews, and suggested improvements to this paper.

Our thanks also go to Professor V. K. Popov for first recommending the Yakutinskaya structure for study, and for his discussions and encouragement, and to Professor S. A. Shcheka for his invaluable advice. We thank Professor Akira Ishiwatari and Professor Hiroaki Sato for their constructive reviews.

Finally, we are grateful to the Japanese Ministry of Education, Culture, Sports, Science and Technology for financial support of a scholarship at Shimane University, Japan.

REFERENCES

Anderson, D.J. and Lindsley, D.H. (1988) Internally consistent solution models for Fe-Mg-Mn-Ti oxides; Fe-Ti oxides. American Mineralogist, 73, 714-726.

Arth, J.G. (1976) Behavior of trace elements during magmatic processes - a summary of theoretical models and their applications. Journal of Research of the US Geological Survey, 4, 41-47.

Baker, D.R. (1989) Tracer versus trace element diffusion: diffusional decoupling of Sr concentration from Sr isotope composition. Geochimica et Cosmochimica Acta, 53, 3015-3023.

Baker, B.H. and McBirney, A.R. (1985) Liquid fractionation. Part III: Geochemistry of zoned magmas and the compositional effects of liquid fractionation. Journal of Volcanology and Geothermal Research, 24, 55-81.

Bence, A.E. and Albee, A.L. (1968) Empirical correction factors for the electron micro-analysis of silicates and oxides. Journal of Geology, 76, 382-403.

Cameron, K.L. (1984) The Bishop Tuff revisited: new rare earth element data consistent with crystal fractionation. Science, 224, 1338-1340.

Carmichael, I.S.E. (1967) The iron-titanium oxides of salic volcanic rocks and their associated ferromagnesian silicates. Contributions to Mineralogy and Petrology, 14, 36-64.

Chapell, B.W. and White, A. (1974) Two contrasting granite types. Pacific Geology, 8, 173-174.

Chesner, C.A. (1998) Petrogenesis of the Toba Tuffs, Sumatra, Indonesia. Journal of Petrology, 39, 3, 397-438.

Cox, K.G., Bell, J.D. and Pankhurst, R.J. (1979) The interpretation of igneous rocks. George Allen & Unwin Ltd. London.

Ferriz, H. and Mahood, G.A. (1987) Strong compositional zonation in a silicic magmatic system: Los Humeros, Mexican Neovolcanic Belt. Journal of Petrology, 28, 171-209.

Frost, B.R., Lindsley, D.H. and Anderson, D.J. (1988) Fe-Ti oxide-silicate equilibria: Assemblages with fayalitic olivine. American Mineralogist, 73, 727-740.

Heumann, A. and Davies, G.R. (1997) Isotopic and chemical evolution of the post-caldera rhyolitic system at Long Valley, California. Journal of Petrology. 38, 12, 1661-1678.

Hildreth, W. (1979) The Bishop Tuff: evidence for the origin of compositional zonation in silicic magma chambers. Geological Society of America. Special Paper, 180, 43-75.

Hildreth, W. (1981) Gradients in silicic magma chambers: Implications for lithospheric magmatism. Journal of Geophysical Research, 86, 10153-10192.

Huppert, H.E. and Sparks, R.S.J. (1984) Double-diffusive convection due to crystallization in magmas. Annual Review of Earth and Planetary Science, 12, 11-37.

Ishihara, S. (1977) The magnetite-series and ilmenite-series granitic rocks. Mining Geology, 27, 293-305.

Johannes, W. and Holtz, F. (1996) Petrogenesis and experimental petrology of granitic rocks. Mineral and rocks, pp.339, Springer-Verlag, Heidelberg.

Kagami, H., Okano, O., Sudo, H. and Honma, H. (1982) Isotope analysis of Rb and Sr using a full automatic thermal ionization mass spectrometer. Okayama Daigaku Onsen Kenkyusho Hokoku, Okayama University, Japan, 52, 54-70.

Kagami, H., Iwata, M., Sano, S. and Honma, H. (1987) Sr and Nd isotopic compositions and Rb, Sr, Sm and Nd concentrations of standard samples. Technical Report of Institute for Study of the Earth's Interior (ISEI), Okayama University, Series. B, 4, 1-16.

Khanchuk, A.I. (1999) A California-type Mesozoic and Cenozoic transform continental margins and associated metallogenesis in the Russian Far East. Geological Society of America, Cordilleran Section, Centennial 1899 - 1999, University of California Berkley, California, Abstracts N 14840. V. 31(6).

Khanchuk, A.I., Ratkin, V.V., Ryazantseva, M.D., Golozubov, V.V. and Gonokova, N.G. (1996) Geology and mineral deposits of Primorsky Krai (Territory). Russian Academy of Sciences, Far East Branch, pp.62, Dalnauka Publishing, Vladivostok.

Kimura, J. and Yamada, Y. (1996) Evaluation of major and trace element XRF analyses using a flux to sample ratio of two to one glass beads. Journal of Mineralogy, Petrology and Economic Geology, 91, 62-72.

Le Bas, M. J., Le Maitre, R. W., Streckeisen, A. and Zanettin, B. (1986) A chemical classification of volcanic rocks based on the total alkali-SiO_2 diagram. The Journal of Petrology, 27, 745-750.

Leake, B.E. (1978) Nomenclature of amphiboles. American Mineralogist, 63, 1023-1052.

Lesher, C.E. (1986) Effects of silicate liquid composition on mineral-liquid element partitioning from soret diffusion studies. Journal of Geophysical Research, 91, 6123-6141.

Lindsley, D.H. (1983) Pyroxene thermometry. American Mineralogist, 68, 477-493.

Lipman, P.W., Christensen, R.L. and O'Connor, J.T. (1966) A compositional zoned ash-flow sheet in southern Nevada. U. S. Geological Survey Professional paper 524-F, pp.47.

Lowell, R.P. (1985) Double-diffusive convection in partially molten silicate systems: Its role during magma generation and in magma chambers. Journal of Volcanological and Geothermal Research, 26, 1-24.

Luth, W.C., Jahns, R.H. and Tuttle, O.F. (1964) The granite system at pressures of 4 to 10 kilobars. Journal of Geophysical Research, 69, 759-773.

Mahood, G.A. and Hildreth, W. (1983) Large partition coefficients for trace elements in high-silica rhyolites. Geochimica et Cosmochimica Acta, 47, 11-30.

Markevich, P.V. (1979) The geochemistry and mineralogy of sedimentary rocks in Russia's far East. pp.183, Far East Geological Institute,Vladivostok (in Russian).

Matyunin, A. P. (1988) Magmatism of the Kavalerovsky and

Verkhnearminskiy tin-bearing areas. Abstract of Ph.D., Far East Geological Institute,Vladivostok, DVGI (in Russian).

Matyunin, A.P., Golozubov, V.V., Lepeshko V.V. and Razmakhnina A.M. (1986) Geological report: Geological structure and useful minerals of Kavalerovsky ore district, Vladivostok (in Russian).

Maury, R. C. and Bizouard, H. (1974) Melting of acid xenoliths into a basanite: an approach to the possible mechanisms of crustal contamination. Contributions to Mineralogy and Petrology, 48, 275-286.

McBirney, A.R., Baker, B.H. and Nilson, R.H. (1985) Liquid fractionation. Part I: Basic principles and experimental simulations. Journal of Volcanology and Geothermal Research, 24, 1-24.

Michael, P.J. (1983) Chemical differentiation of the Bishop tuff and other high-silica magmas through crystallization processes. Geology, 11, 31-34.

Mikhailov, V.A. (1989) The magmatism of volcanotectonic structures in the southern segments of the East Sikhote-Alin volcanic belt. pp.172, Far East Branch Russian Academy of Science, Vladivostok (in Russian).

Miyashiro, A. (1978) Nature of alcalic volcanic rock series. Contributions to Mineralogy and Petrology, 66, 91-104.

Nilson, R.H., McBirney, A.R. and Baker, B.H. (1985) Liquid fractionation. Part II: Fluid dynamics and quantative implications for magmatic systems. Journal of Volcanology and Geothermal Research, 24, 25-54.

Noble, D.C. and Hedge, C.E. (1969) $^{87}Sr/^{86}Sr$ variations within individual ash-flow sheets. U.S. Geological Survey Professional Paper, 650-C: 133-139.

Obata, M., Banno, S. and Mori, T. (1974) The iron-magnesium partitioning between naturally occurring coexisting olivine and Ca-rich clinopyroxene: an application of the simple mixture model to olivine solid solution. Bulletin de la Société Française de Minéralogie et de Cristallographie, 97, 101-107.

Pankhurst, R.J. (1969) Strontium isotope studies related to petrogenesis in the Caledonian basic igneous province of NE Scotland. Journal of Petrology, 10, 115-143.

Popov, V.K. and Grebennikov, A.V. (1997) Geological and geochemical correlation of rhyolites from the Yakutinskaya and Avgustovskaya volcanic structures, Primorye. Geology of Pacific Ocean, 13, 583-600.

Shaw, H.R., Smith, R.L. and Hildreth, W. (1976) Thermogravitational mechanisms for chemical variations in zoned magma chambers. Abstracts with Programs of Geological Society of America Annual Meeting, 8, the Geological Society of America, Boulder, CO, 1102.

Smith, R. (1979) Ash-flow magmatism. Geological Society of America. Special Paper, 180, 5-27.

Smith, R.L. and Bailey, R.A. (1966) The Bandelier Tuff: A study of ash-flow eruption cycles from zoned magma chambers. Bulletin Volcanologique, 29, 83-104.

Turner, J.S. and Campbell, I.H. (1986) Convection and mixing in magma chambers. Earth-Science Reviews, 23, 255-352.

Tuttle, O.F. and Bowen, N.L. (1958) Origin of granite in the light of experimental studies in the system $NaAlSi_3O_8$-$KalSi_3O_8$-SiO_2-H_2O. Geological Society of America, Memoir 74: pp.154.

Watson, E.B. (1982) Basalt contamination by continental crust: Some experiments and models. Contributions to Mineralogy and Petrology, 80, 73-87.

Williams, H. (1942) The geology of Crater Lake National Park, Oregon, with a reconnaissance of the Cascade Range southward to mount Shasta. Carnegie Institution of Washington Publication, 540, pp.162.

York, D. (1969) Least-squares filling of a straight line with correlated errors. Earth and Planetary Science Letters, 5, 320-324.

Manuscript received January 27, 2005
Manuscript accepted October 28, 2005
Manuscript handled by Hirokazu Fujimaki